Supporting Information

Boyer et al. 10.1073/pnas.0911354106

SI Text

SI Methods. *Analysis of Marseillevirus genome.* Protein-coding genes were predicted using GeneMark.hmm 2.0 (1) with the following modifications: (*i*) eight short (<50 aa) sequences with no matches in the NCBI Refseq database (2) were eliminated; and (*ii*) intergenic spaces were screened using BLASTX against Refseq database to identify potential missed genes and gene fragments; all ORFs were searched against the Refseq to check gene boundaries; as a result, in 28 cases, ORF boundaries were manually corrected.

The 457 translated protein sequences were searched against the NCBI Refseq and env_nr (environmental nonredundant) protein sequence databases using BLASTP (3). Conserved domains were identified by searching the Conserved Domain Database (CDD version 2.13) (4) using RPS-BLAST. Best Refseq hits and identified conserved domains were used to annotate 219 Marseillevirus proteins.

Marseillevirus protein families (28 clusters of paralogs) were delineated by similarity-based clustering of Marseillevirus protein sequences using BLASTCLUST with subsequent manual curation. The 17 genes unique (amongst NCLDVs) to Mimivirus and Marseillevirus were identified by analysis of phyletic patterns.

Proteins with putative homologs in Refseq were composed of two categories: (*i*) proteins with best Refseq hits e-values ≤0.0001 (161 proteins), and (*ii*) proteins with best Refseq hits E-values between 0.0001 and 0.01. All of the proteins in the second category were examined case by case, and 27 of the 64 were included in the set of evolutionarily conserved proteins of Marseillevirus. Thus, 188 proteins were defined as having homologs in Refseq and used for detailed analysis described below.

Acanthamoeba castellanii Neff draft genome was downloaded from the Human Genome Sequencing Center at Baylor College of Medicine FTP site (ftp://ftp.hgsc.bcm.tmc.edu/pub/data/AcastellaniNeff/). Marseillevirus proteins were searched against the *Acanthamoeba castellanii* nucleotide sequences using TBLASTN; for significant hits, *Acanthamoeba* protein fragments were collected directly from the BLAST output. Of the 188 Marseillevirus proteins used for the analysis, 80 had one or more homologs in *Acanthamoeba*.

Each of the 188 Marseillevirus proteins was aligned (MUSCLE; ref. 5) with the following sequences: the top Refseq and environmental hits (clustered by BLASTCLUST if numerous); NCLDV othologous proteins (if relevant); and *Acanthamoeba* hits (if any). Closely related Marseillevirus proteins were included in the same alignments. Alignments were edited as follow: short sequences (mainly environmental sequences) and sequences that did not match most conserved positions of the alignment were removed manually; gapped and less conserved positions were removed either automatically or manually. Maximum-likelihood trees were built from the alignments whenever possible (that is, except for the cases with too few Refseq homologs or too few informative positions). Maximum-likelihood trees were constructed using the TreeFinder program (6), with the estimated site rates heterogeneity and with the WAG (Whelan and Goldman) substitution model (7). The expected-likelihood weights of 1,000 local rearrangements were used as confidence values of TreeFinder tree branches (8).

The phyletic patterns indicating the presence/absence of the respective gene in each species were used for the construction of the neighbor-joining tree shown in Fig. 4 (phylip3.66; ref. 9).

Sequences of the different primers used in RT-PCR analysis. RNA was extracted from purified virions and submitted to RT-PCR analysis using a subset of virus-specific primers: ORF329 was amplified with primers DNA_polT19F (5′-CGAAGCGTACTCGAAGAACC-3′) and DNA_polT19R (5′-AGACGCTTCTCTGTCGGGTA-3′), ORF157 with primers A32_ATPase_T19F (5′-TCCGCTTCCTATTTTGTGCT-3′) and A32_ATPase_T19R (5′-TAGGATGAGGGGCACGATAC-3′), ORF270 with primers A18_helicaseF (5′-CAGAACTCCGTGCTCTTTCC-3′) and A18_helicaseR (5′-CGCTCTTCCCTCGTACTGAC-3′), ORF342 with primers capsid_T19F (5′-TAACTGCTGCTTCCGGTTTT-3′) and capsid_T19R (5′-ATCTCCGGAACGATTCACAG-3′), ORF310 with primers Thiol_ox_T19F (5′-AGAACCACAAGCTCCTCGAA-3′) and Thiol_ox_T19R (5′-GAAATTTGCCCTGCAAGAAA-3′), ORF203 with primers D6R_helic_T19F (5′-GGCAGTGAGGTTTTGCTCTC-3′) and D6R_helic_T19R (5′-CAACAGCGGCTTCTTTTAGG-3′), ORF424 with primers S/T_kinase_T19F (5′-GCATCCAAAAATCTCCTCCA-3′) and S/T_kinase_T19R (5′-GCAACCCGCATATTTTCTGT-3′), ORF237 with primers A1L-TF_T19F (5′-AACCGCGGTACTGATGAAAG-3′) and A1L-TF_T19R (5′-TTTGTGGTCTGTTGGGAGGT-3′), ORF213 with primers TFIIB_T19F (5′-TTCGGTCCCAAAAGAACTTG-3′) and TFIIB_T19R (5′-GTGCAAACGATGATGACACC-3′), ORF166 with primers Histone2A_T19F (5′-CAACATGCTCGTGTTTTTGG-3′) and Histone2A_T19R (5′-TTTTTGTGGGGAAAACAAGC-3′), and ORF414 with primers histoneH2B_T19F (5′-CAGAAGTTCAAAGGCCAAGC-3′) and histoneH2B_T19R (5′-TTCGCACCTTCTTCGAATCT-3′). Amoeba 18S rRNA gene was amplified with forward primer 5′-AACGAAAGTTAGGGGATCGAA-3′ and reverse primer 5′-ACAAGCTGCTAGGGGAGTCA-3′.

SI Results. ***Kinetics and quantification of Marseillevirus replication cycle.*** The main morphological changes along the replication cycle were studied by direct DNA staining with DAPI (10) of *A. castellanii* infected cells at different time points p.i. or uninfected, as negative controls. The observed changes concerned VF formation and host cell nucleus modifications. Results are shown in Fig. S5. Fluorescence microscopy pictures showed VF brightly stained at 3 h 30 min p.i. that continued to grow until 6 h 30 min p.i. VF formation kinetics was quantified by using the integrated DAPI fluorescence intensity and varied up to 2.5×10^6 times compared with negative controls (circle curve), whereas there was no significant variation of staining in infected cell nuclei compared to control cells (diamond curve). However, infected cell nuclei underwent a strong but transient morphological modification between 30 min and 2 h 30 min p.i. observed by fluorescence microscopy. Variation of host cell nucleus morphology was quantified using two parameters: the heterogeneity of DAPI staining (black bar histogram) and the ratio between the number of nuclei with a standard ring-like morphology over the total number of nuclei in the microscope field (white bar histogram). For uninfected control cells this ratio was of 60.3%. For these parameters, findings are shown as a percent variation compared with the uninfected cells. As soon as 30 min p.i., only 18% infected cells showed the nucleus ring-like morphology, whereas at 4 h 30 min p.i., 74% of infected cells recovered this morphology. In the meantime, an increase in DAPI staining heterogeneity (up to 172.8% at 30 min and 111.4% at 4 h 30 min versus 100% for the control cells) (black bar histogram) was observed. The measures were limited to 4 h

30 min p.i. due to the difficulty of clearly identifying the nuclei in amoebae harboring very large and bright VF. Thus Marseillevirus replication cycle shares common features with that of Mimivirus as to interaction with cell nuclei, formation, and growth of an independent VF, but has also specificities such as VF morphology, growth kinetics, synthesis, and assembly of progeny virions.

Detection of viral RNA within Marseillevirus particles. Cellular DNA and RNA contamination was excluded because no 18S amplification product could be detected after PCR and RT-PCR on RNA isolated from purified Marseillevirus. RNA samples were free of Marseillevirus DNA contamination because no amplified product was observed after RT-PCR using Taq polymerase instead of the RT/Taq enzyme mix. Transcripts of genes coding respectively for DNA polymerase (ORF329), capsid protein (ORF342), TFII-like transcription factor (ORF213), and D6R helicase (ORF203) have been detected with specific amplification of cDNA obtained after reverse transcription of viral RNA, suggesting that viral transcripts might be packaged in Marseillevirus particles.

Coinfection of* A. castellanii *with purified Marseillevirus,* Legionella drancourtii, *and* Parachlamydia *strain BN9. *A. castellanii* were infected with a mixture of Marseillevirus, *Legionella drancourtii*, and *Parachlamydia* strain BN9. At 16 and 24 h p.i., amoebal cells were spotted on microscopes slides using a Cytospin. Then, nucleic acids were stained using DAPI (Molecular Probes) or Hemacolor (Merck), according to the manufacturer's instructions. The morphology of each DAPI or Hemacolor-stained microorganism inside the amoebal cells was identified by comparison with amoeba infections with each microorganism alone. As shown in Fig. 5, VF of Marseillevirus, strongly stained with DAPI (Fig. 5*A Left*) or with Hemacolor (purple color) (Fig. 5*A Right*), can coexist in the same amoebal cytoplasm with both *Legionella drancourtii* (long rod-shaped bacteria, blue colored in Hemacolor staining) and *Parachlamydia* (coccoid-shaped bacteria, blue-colored in hemacolor staining). Thus, coinfected amoebal cells could be the host for simultaneous bacteria and virus multiplication.

1. Lukashin AV, Borodovsky M (1998) GeneMark.hmm: New solutions for gene finding. *Nucleic Acids Res* 26:1107–1115.
2. Pruitt KD, Tatusova T, Klimke W, Maglott DR (2009) NCBI Reference Sequences: Current status, policy and new initiatives. *Nucleic Acids Res* 37:D32–D36.
3. Altschul SF, et al. (1997) Gapped BLAST and PSI-BLAST: A new generation of protein database search programs. *Nucleic Acids Res* 25:3389–3402.
4. Marchler-Bauer A, et al. (2009) CDD: Specific functional annotation with the Conserved Domain Database. *Nucleic Acids Res* 37:D205–D210.
5. Edgar RC (2004) MUSCLE: Multiple sequence alignment with high accuracy and high throughput. *Nucleic Acids Res* 32:1792–1797.
6. Jobb G, von Haeseler A, Strimmer K (2004) TREEFINDER: A powerful graphical analysis environment for molecular phylogenetics. *BMC Evol Biol* 4:18.
7. Whelan S, Goldman N (2001) A general empirical model of protein evolution derived from multiple protein families using a maximum-likelihood approach. *Mol Biol Evol* 18:691–699.
8. Strimmer K, Rambaut A (2002) Inferring confidence sets of possibly misspecified gene trees. *Proc Biol Sci* 269:137–142.
9. Felsenstein J (2005) PHYLIP (Phylogeny Inference Package), version 3.6. Distributed by the author. (Department of Genome Sciences, University of Washington, Seattle).
10. Suzan-Monti M, La Scola B, Barrassi L, Espinosa L, Raoult D (2007) Ultrastructural characterization of the giant volcano-like virus factory of *Acanthamoeba polyphaga Mimivirus*. *PLoS One* 2:e328.

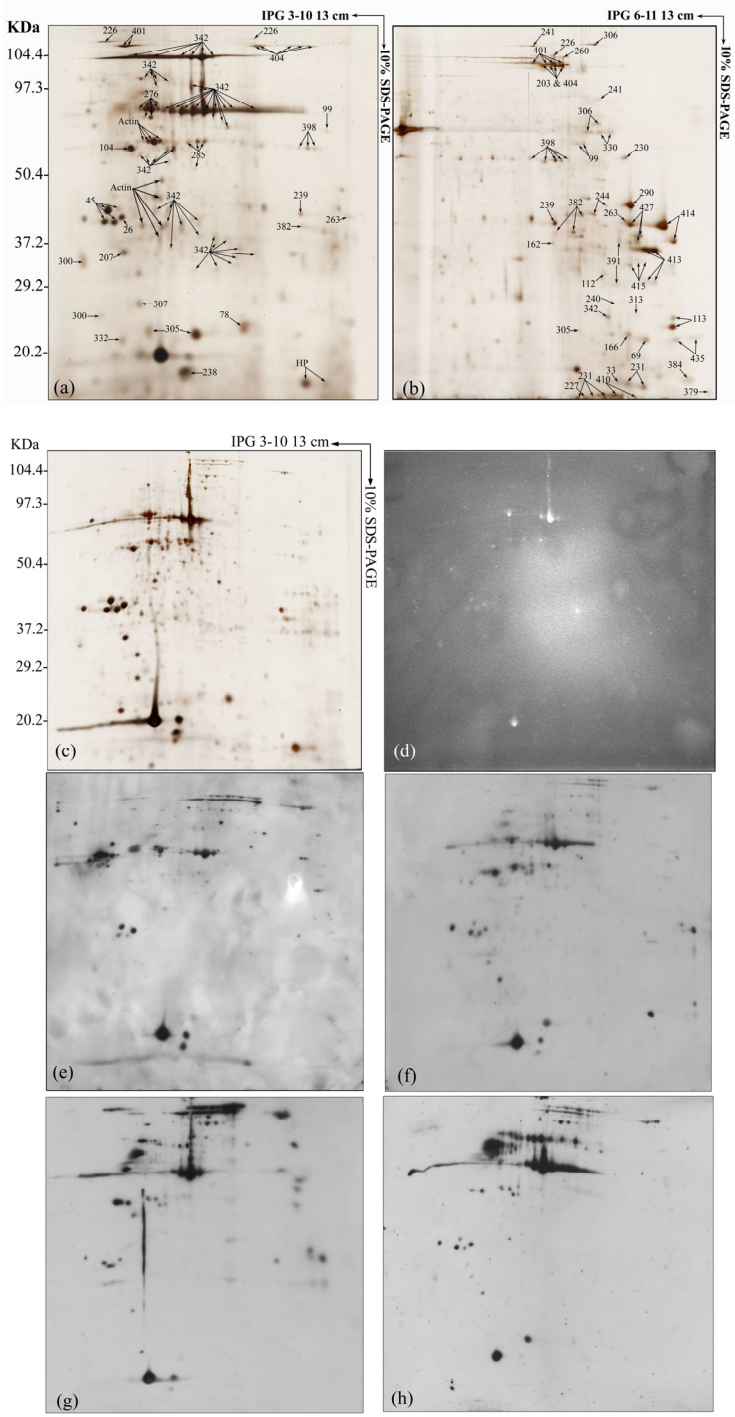

Fig. S1. (*a* and *b*) 2D reference gels of the protein extract of Marseillevirus. Proteins were resolved in the first dimension over a pI gradients of 3–10 (*a*) or 6–11 (*b*), followed by 10% linear SDS/PAGE for the second-dimension separation. The 2D gels were silver stained. Identified proteins, achieved by MALDI-TOF analysis, are indicated by arrows and listed in .pdf;2009_PDF;/Border [0 0 0]Table S1. Standard molecular weight and p*I* range are indicated. HP corresponds to ORF product not detected during ORF prediction. Actin spots correspond to actin proteins from host cells. (*c*–*h*) Posttranslational analysis of Marseillevirus proteins resolved on 2D gel. Viral proteins resolved by 2D gels were revealed by silver staining (*c*). Glycoproteins were stained with the Pro-Q Emeral 300 glycoprotein kit according to the manufacturer's protocol (*d*). Western blot analysis using the mouse polyclonal antiserum (1/2,500) prepared against purified viral particles is shown in (*e*). Phosphorylated proteins were revealed with anti-phosphoserine (1/10,000) (*f*), anti-phosphothreonine (1/10,000) (*g*), or anti-phosphotyrosine (1/10,000) (*h*) mAbs. Standard molecular weight markers are indicated on the left.

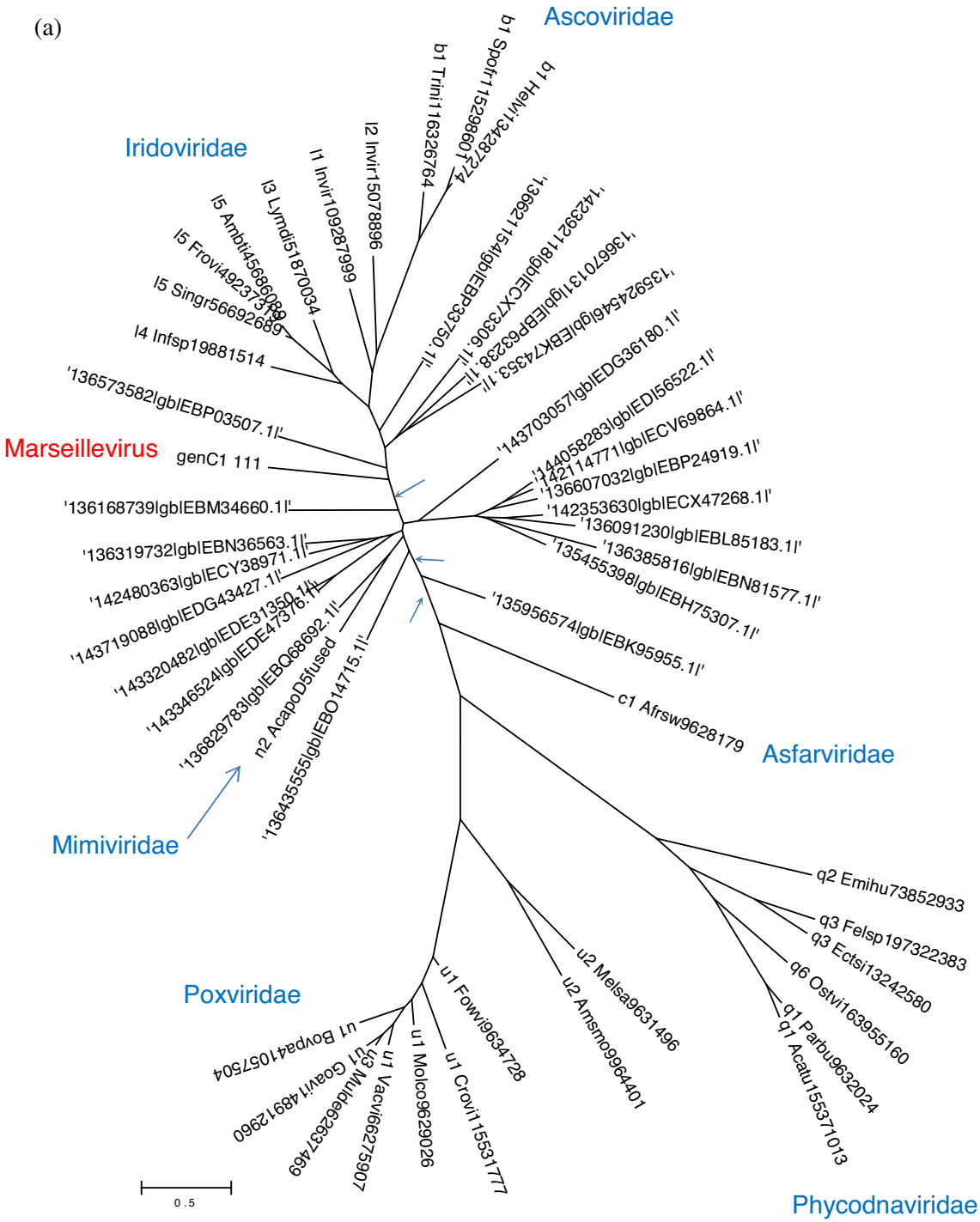

Fig. S2. Phylogenetic analysis of conserved NCLDV proteins: (*a*) D5-like helicase; (*b*) DNA polymerase; (*c*) A32-like ATPase; (*d*) major capsid protein; (*e*) VLTF2-like transcription factor; (*f*) A18-like helicase. Maximum-likelihood (ML) trees were constructed using the TreeFinder program, with the estimated site rates heterogeneity and with the WAG substitution model. The expected-likelihood weights of 1,000 local rearrangements were used as confidence values of TreeFinder tree branches. Reference strains used: b1_Helvi, *Heliothis virescens* ascovirus 3e; b1_Spofr, *Spodoptera frugiperda* ascovirus 1a; b1_Trini, *Trichoplusia ni* ascovirus 2c; c1_Afrsw, African swine fever virus; I1_Invir, Invertebrate iridescent virus 3; I2_Invir, Invertebrate iridescent virus 6; I3_Lymdi, Lymphocystis disease virus - isolate China; I5_Ambti, *Ambystoma tigrinum* virus; I5_Frovi, Frog virus 3; I5_Singr, Singapore grouper iridovirus; n2_Acapo, *Acanthamoeba polyphaga* mimivirus; q1_Acatu, *Acanthocystis turfacea Chlorella* virus 1; q1_Parbu, *Paramecium bursaria Chlorella* virus 1; q2_Emihu, *Emiliania huxleyi* virus 86; q3_Ectsi, *Ectocarpus siliculosus* virus 1; q3_Felsp, Feldmannia species virus; q6_Ostvi, *Ostreococcus* virus OsV5; u1_Bovpa, Bovine papular stomatitis virus; u1_Crovi, Crocodilepox virus; u1_Ectvi, Ectromelia virus; u1_Fowvi, Fowlpox virus; u1_Goavi, Goatpox virus Pellor; u1_Molco, Molluscum contagiosum virus; u2_Amsmo, *Amsacta moorei* entomopoxvirus; u2_Melsa, *Melanoplus sanguinipes* entomopoxvirus; u3_Mulde, Mule deer poxvirus. Environmental sequences are named by their GenBank accession numbers.

(b)

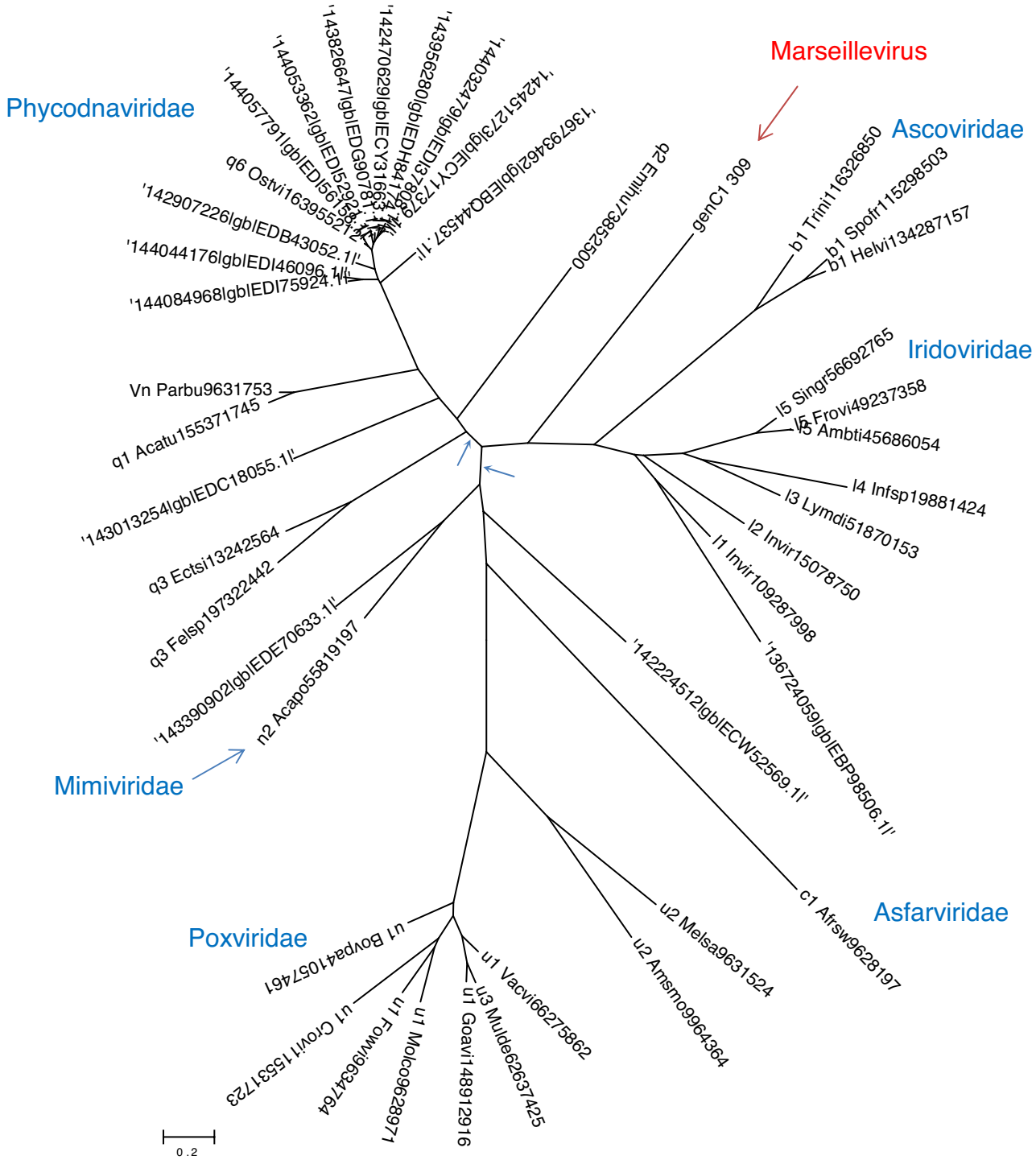

Fig. S2. Continued.

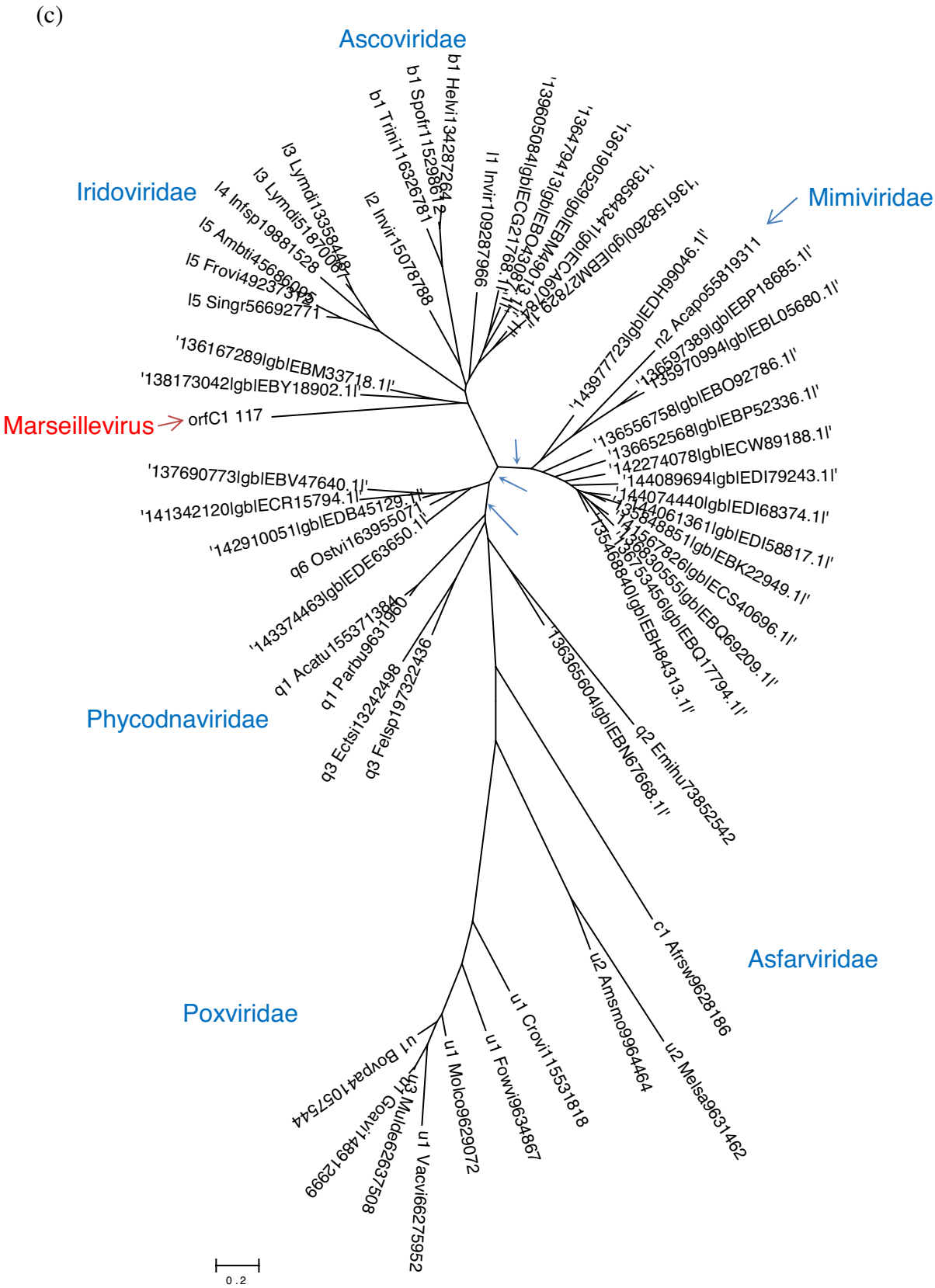

Fig. S2. Continued.

(d)

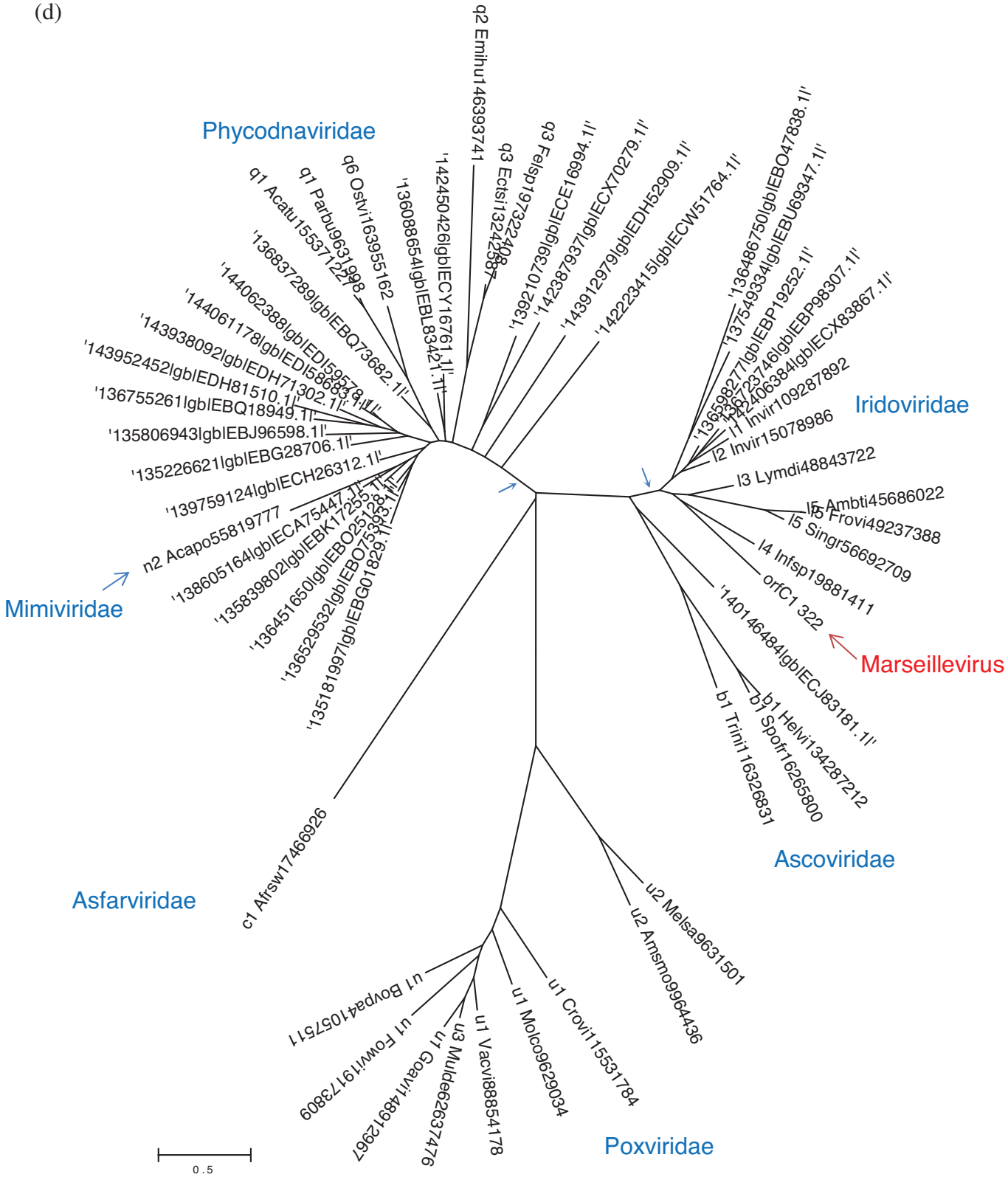

Fig. S2. Continued.

(e)

Fig. S2. Continued.

(f)

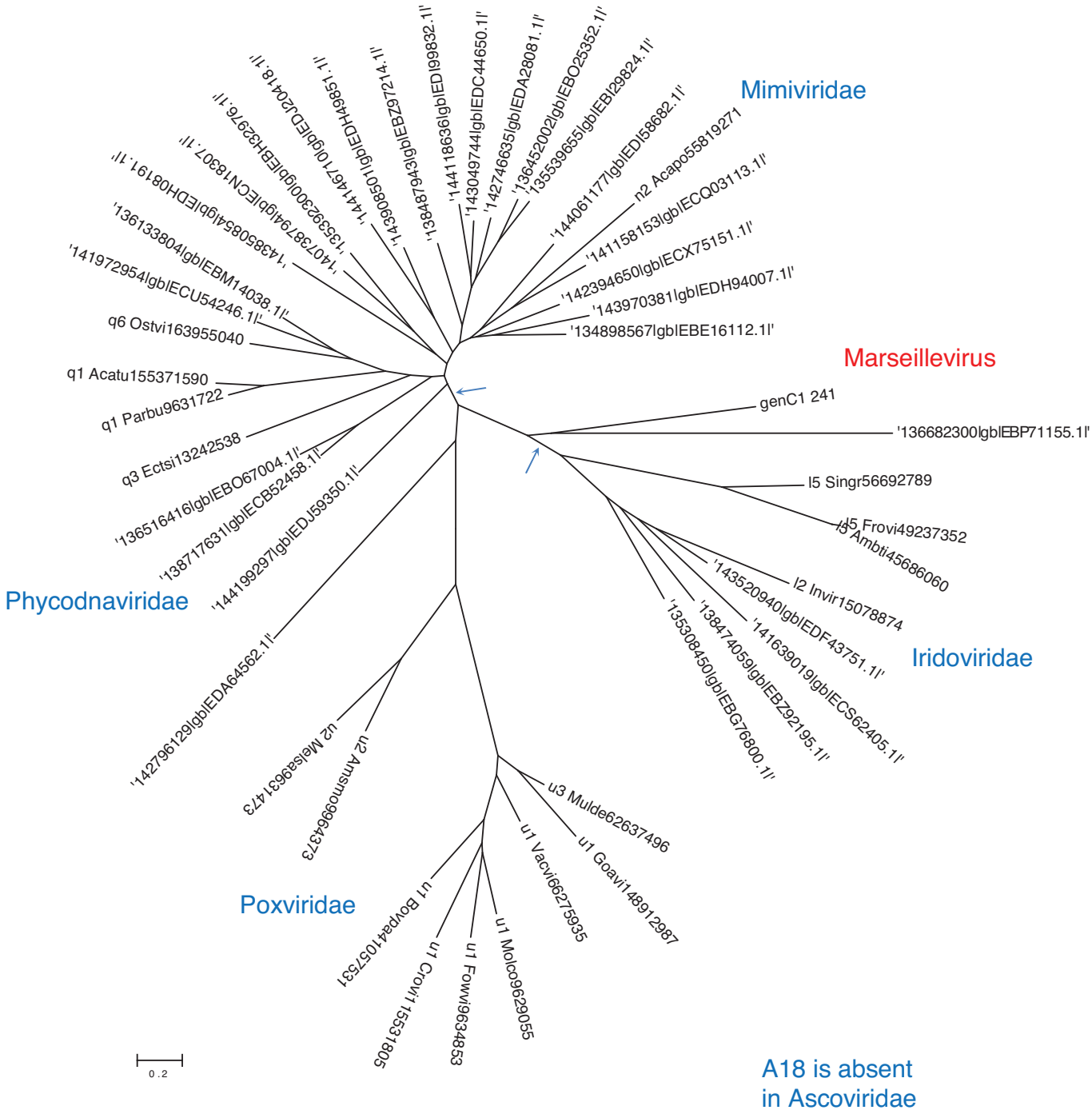

Fig. S2. Continued.

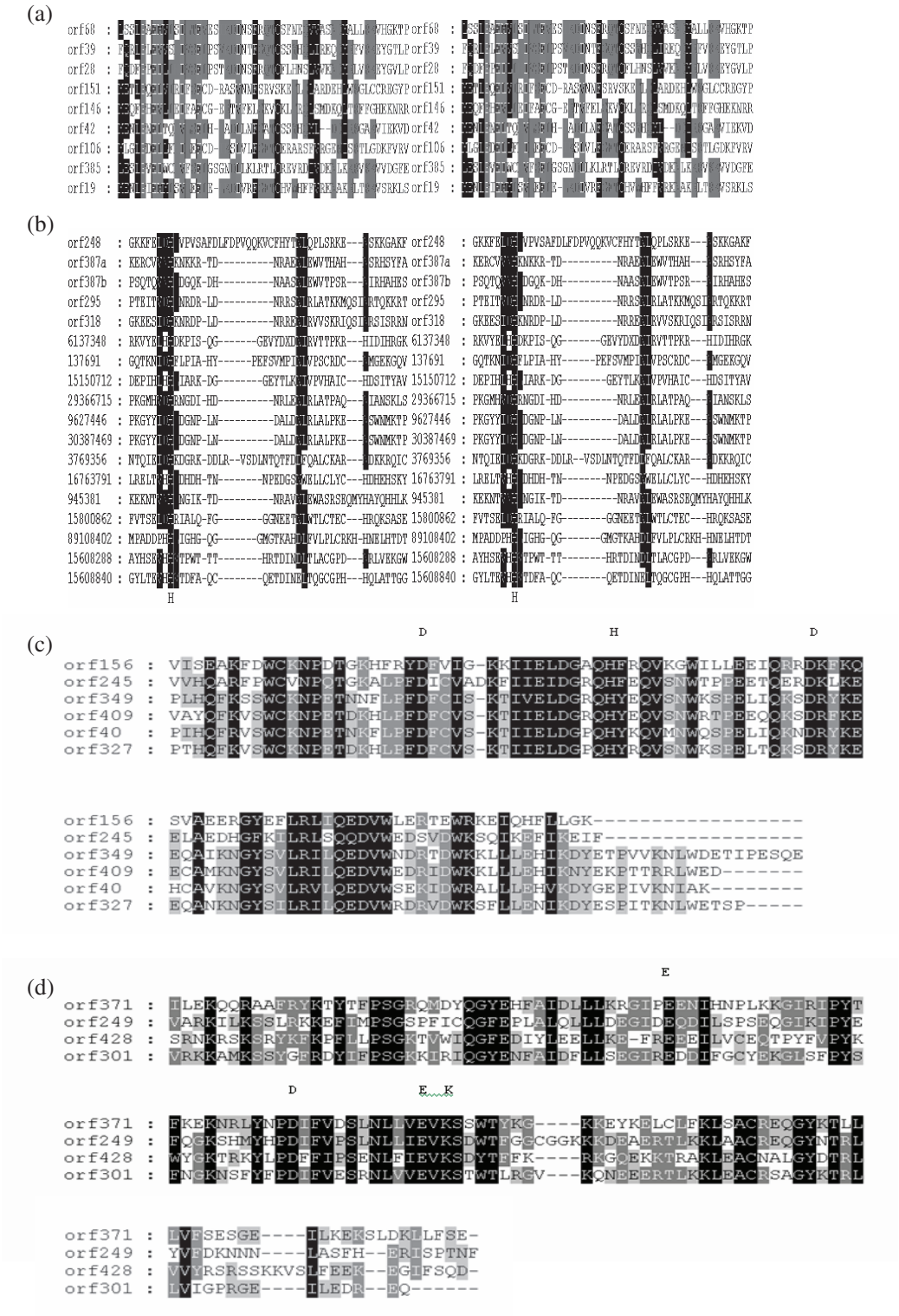

Fig. S3. (*a*) Alignment of the F-box from nine F-box-containing proteins found in Marseillevirus. (*b*) Five Marseillevirus HNH endonuclease domains aligned with GenBank representatives: 6137348, pdb 1BXI_B, *Escherichia coli*; 137691, *Enterobacteria* phage lambda; 15150712, *Pylaiella littoralis*; 29366715, *Pseudomonas* phage gh-1; 9627446, *Enterobacteria* phage T7; 30387469, *Yersinia* pestis phage phiA1122; 3769356, *Helicobacter pylori*; 16763791, *Salmonella typhimurium* LT2; 945381, *Lactobacillus* phage LL-H; 15800862, *Escherichia coli* O157:H7; 89108402, *Escherichia coli* W3110; 15608288, *Mycobacterium tuberculosis* H37Rv; 15608840, *Mycobacterium tuberculosis* H37Rv. (*c* and *d*) Alignment of restriction endonuclease-like proteins found in Marseillevirus. (*c*) Cluster 4 (eight proteins). (*d*) Cluster 10 (four proteins). The positions conserved in cd01038 (*c*) and in cd00523 (*d*) are indicated in the row above the alignment. The alignment was done by MUSCLE and edited manually.

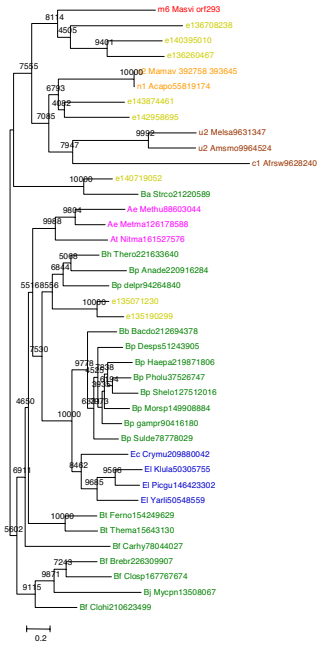

Fig. S4.1. AP (apurinic) endonuclease family 2 (Marseillevirus orf293)

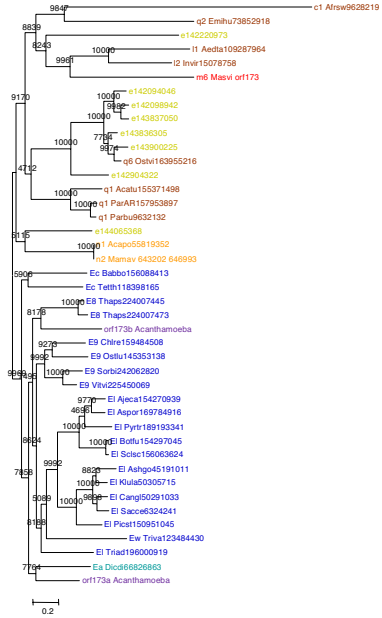

Fig. S4.2. DNA topoisomerase II (Marseillevirus ORF173)

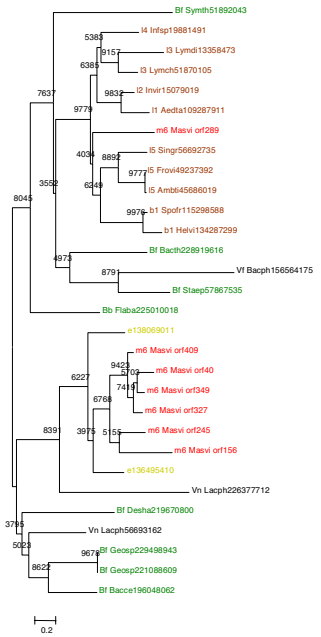

Fig. S4.3. Restriction endonuclease (Marseillevirus ORF156)

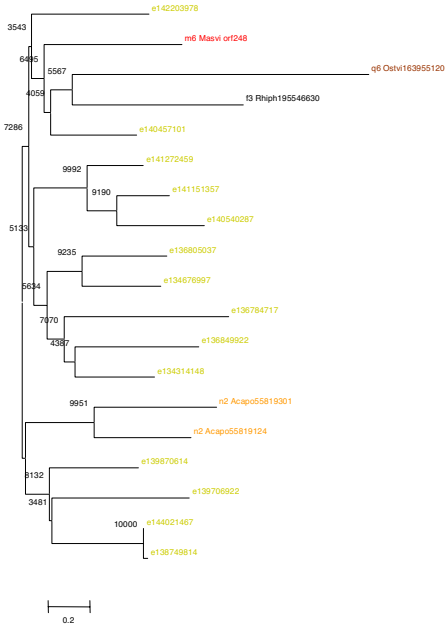

Fig. S4.4. HNH family endonuclease (Marseillevirus ORF248)

Fig. S4. (see Fig. S4.1–S4.89). Phylogenetic trees were constructed for 22 Marseillevirus proteins involved in DNA replication, recombination, and repair (Fig. S4.1–S4.22); 9 in nucleotide metabolism (Fig. S4.23–S4.31); 12 in signaling (Fig. S4.32–S4.43); 10 in protein and lipid synthesis, modification, and degradation (Fig. S4.44–S4.53); 16 in transcription and chromatin modification (Fig. S4.54–S4.69); 5 in translation (Fig. S4.70 to S4.74); 8 in miscellaneous functions (Fig. S4.75–S4.82); and 7 of unknown function (Fig. S4.73–S4.89). A color code was used to represent taxonomic groups, *Bacteria* in green, *Archaea* in pink, *Acanthamoeba* in purple, *Dictyostelium* in green-blue, *Entamoeaba* in light blue, other eukaryotes in dark blue, Mimiviruses in orange, Marseillevirus in red, other NCLDVs in brown, other viruses and phages in dark, and environmental sequences in yellow. Maximum-likelihood trees were constructed using the TreeFinder program, with the estimated site rates heterogeneity and with the WAG (Whelan and Goldman) substitution model. The expected weights of 1,000 local rearrangements were used as confidence values of TreeFinder tree branches.

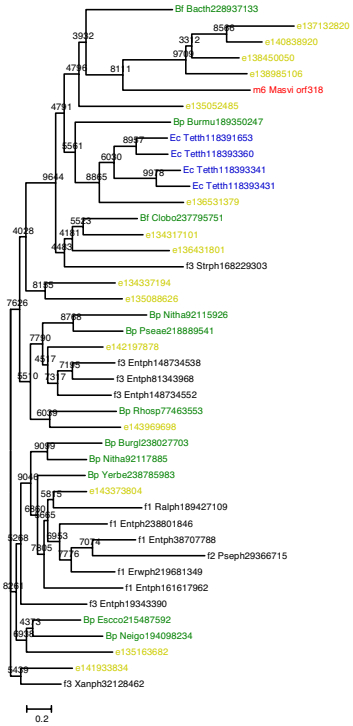

Fig. S4.5. HNH family endonuclease (Marseillevirus ORF318)

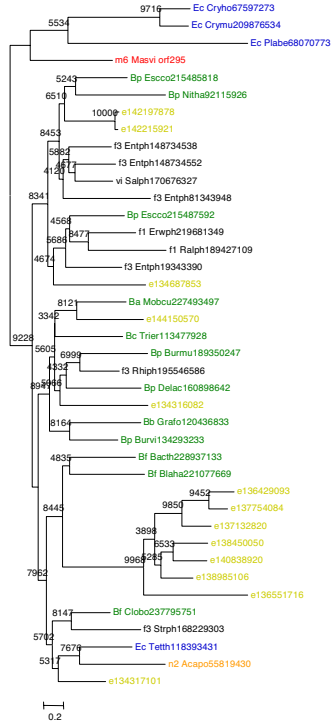

Fig. S4.6. HNH family endonuclease (Marseillevirus ORF295)

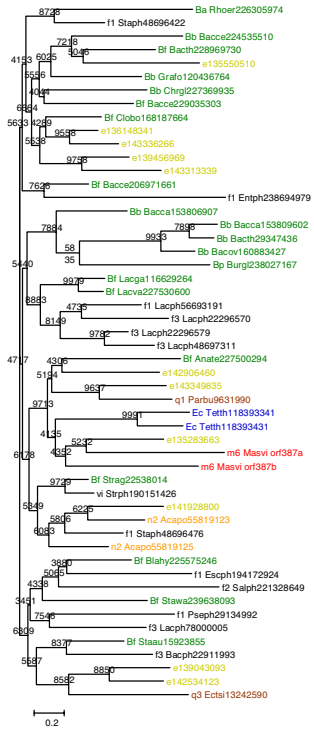

Fig. S4.7. HNH family endonuclease (Marseillevirus ORF387)

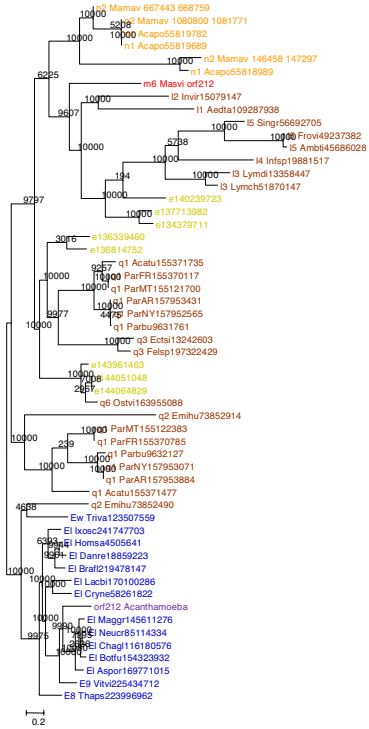

Fig. S4.8. Proliferating Cell Nuclear Antigen (PCNA) (Marseillevirus ORF212)

Fig. S4. Continued.

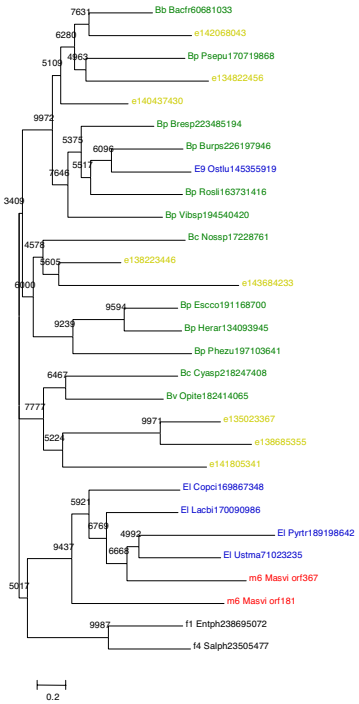

Fig. S4.9. putative nuclease linked to bacterial restriction-modification systems (Marseillevirus ORF181)

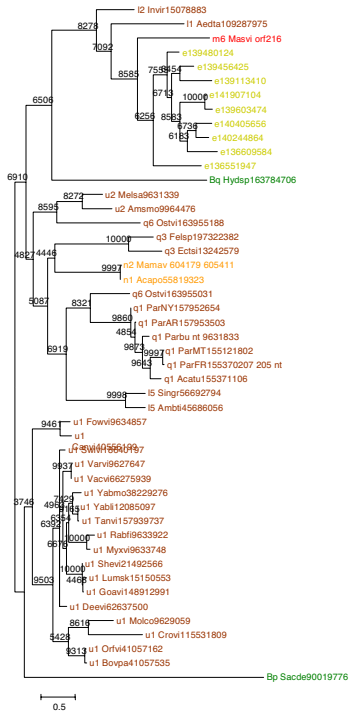

Fig. S4.10. RuvC-like Holiday Juncition Resolvase (Marseillevirus ORF216)

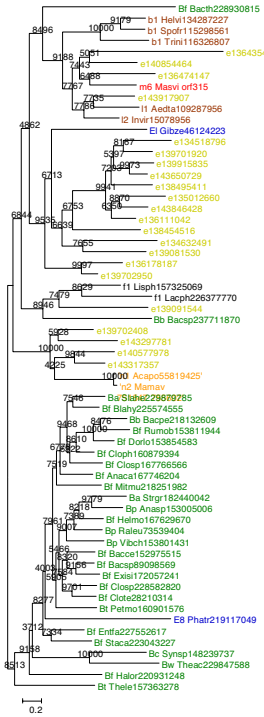

Fig. S4.11. DNA repair exonuclease SbcCD,D subunit (Marseillevirus ORF315)

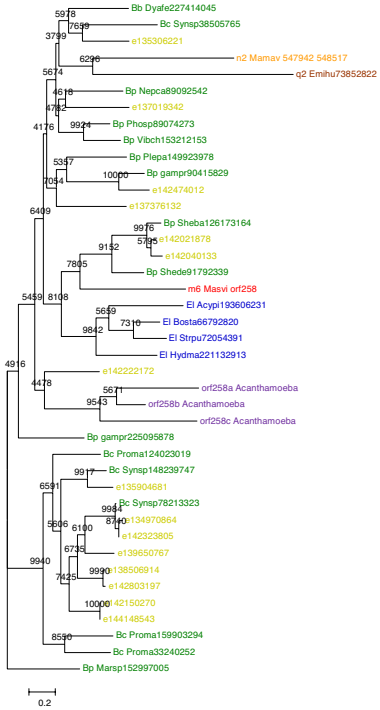

Fig. S4.12. AlkB, Alkylated DNA repair protein unique in NCLDV (Marseillevirus ORF258)

Fig. S4. Continued.

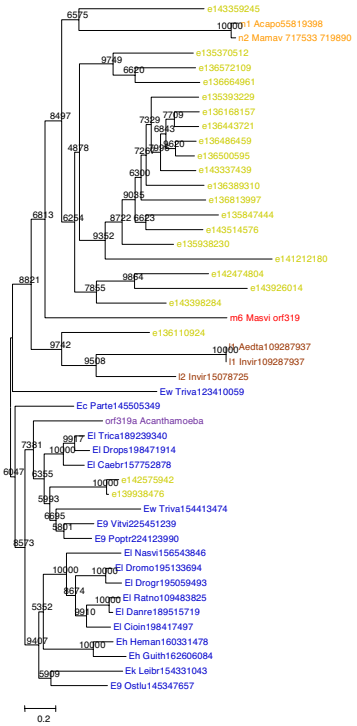

Fig. S4.13. XRN1, 5'-3' exonuclease (Marseillevirus ORF319)

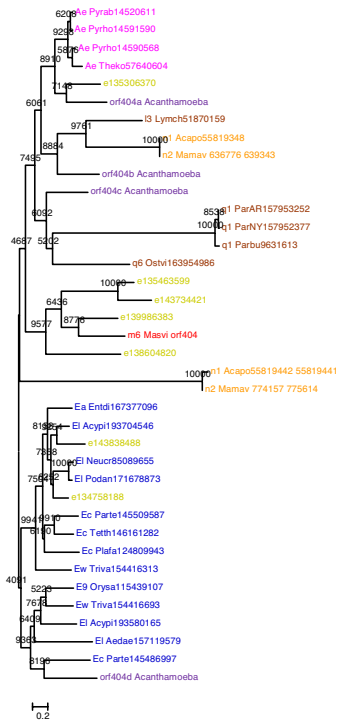

Fig. S4.14. AAA family ATPase (Marseillevirus ORF404)

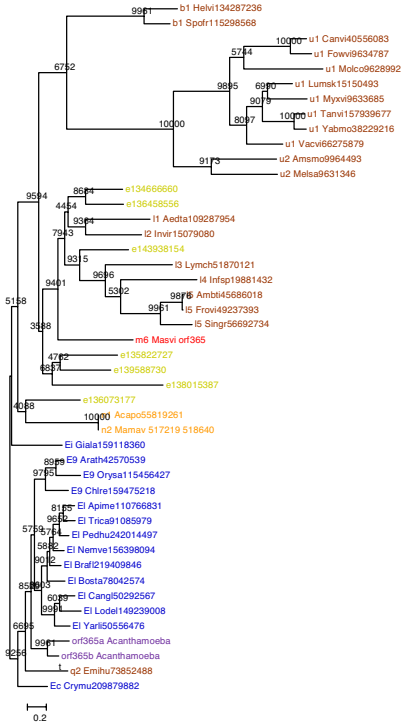

Fig. S4.15. flap-specific endonuclease (poxvirus G5 homolog) (Marseillevirus ORF365)

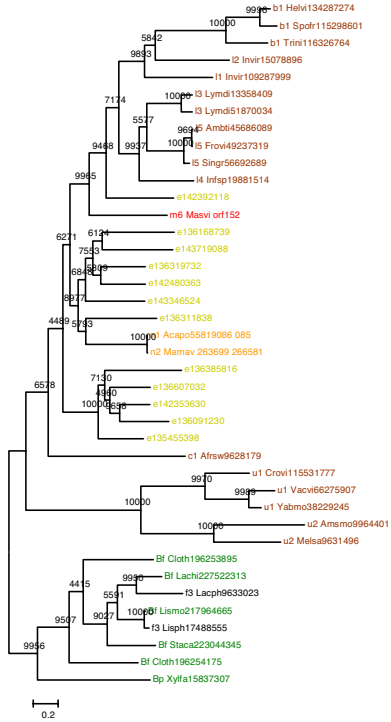

Fig. S4.16. D5 family helicase-primase (Marseillevirus ORF152)

Fig. S4. Continued.

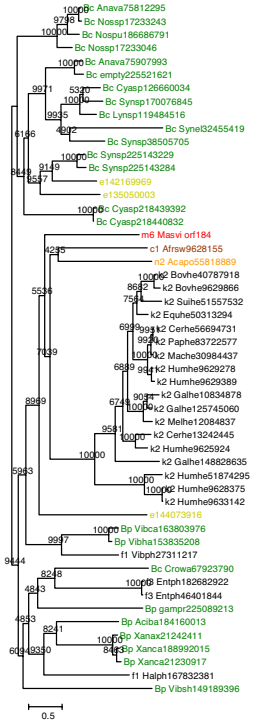

Fig. S4.17. helicase origin-binding-protein (UL9) like (Marseillevirus ORF184)

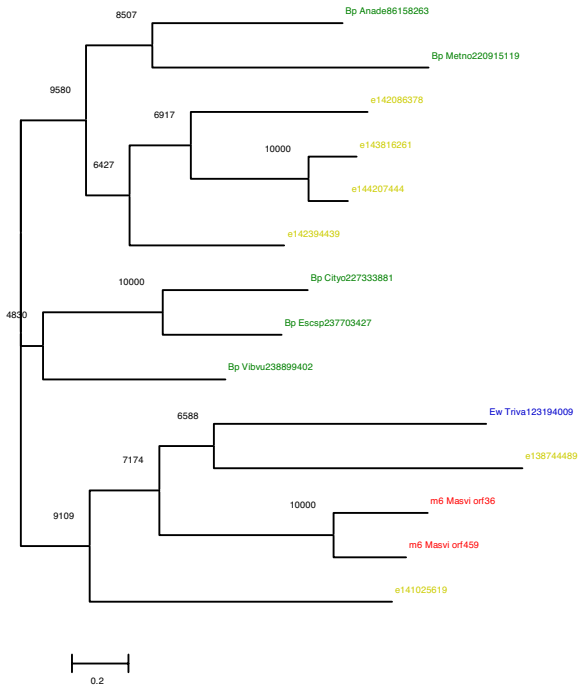

Fig. S4.18. Highly derived D5-like helicase-primase (Marseillevirus ORF36)

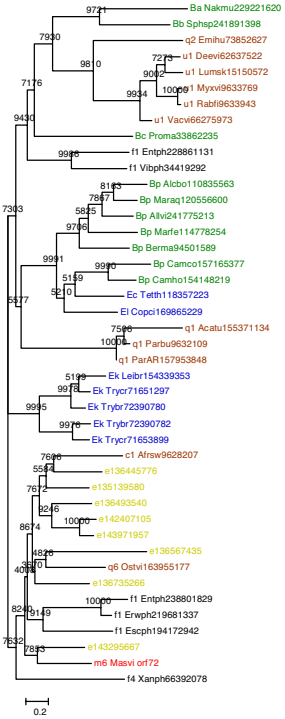

Fig. S4.19. ATP-dependent DNA ligase (Marseillevirus ORF72)

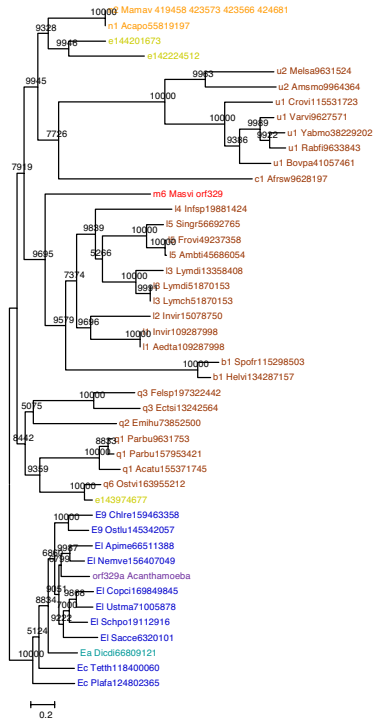

Fig. S4.20. DNA polymerase elongation subunit (family B) (Marseillevirus ORF329)

Fig. S4. Continued.

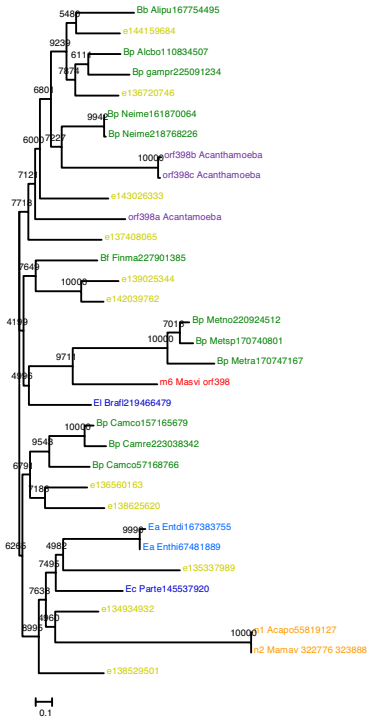

Fig. S4.21. uracil-DNA glycosylase, D4 (Marseillevirus ORF398)

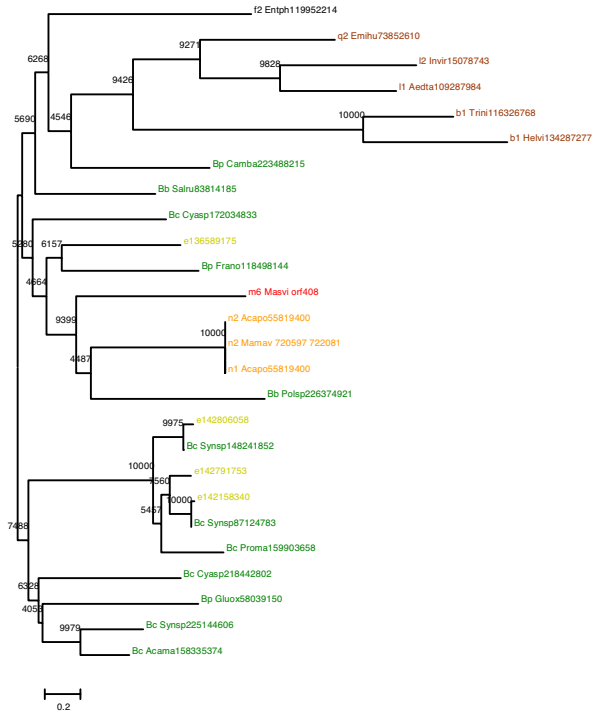

Fig. S4.22. helicase superfamily I member (RecD, ATP-dependent exoDNAse (exonuclease V), alpha subunit) (Marseillevirus ORF408)

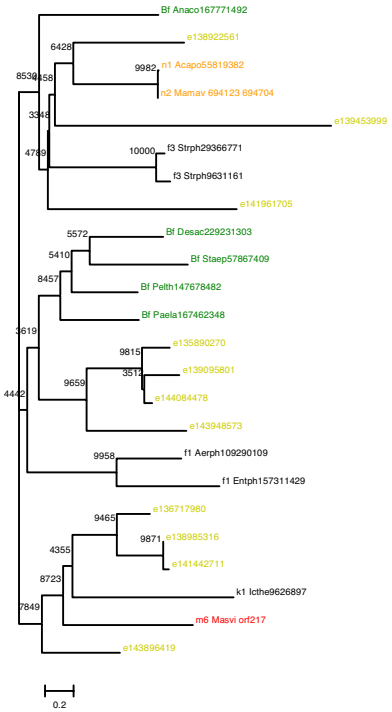

Fig. S4.23. dNMP kinase (Marseillevirus ORF217)

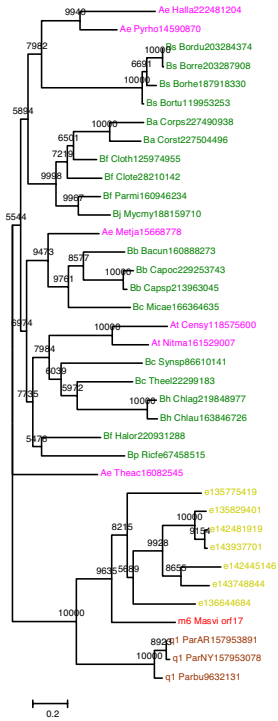

Fig. S4.24. Dam-like adenine-specific DNA methylase (Marseillevirus ORF17)

Fig. S4. Continued.

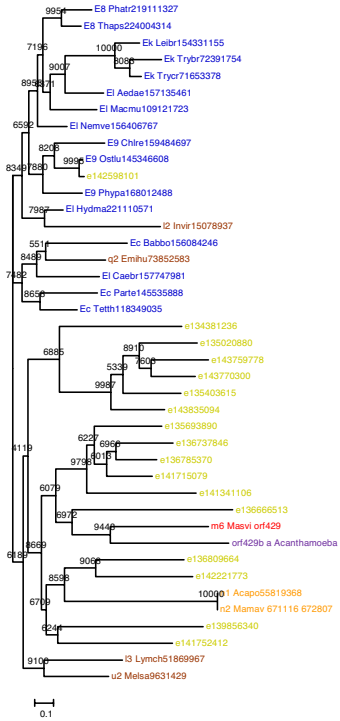

Fig. S4.25. bifunctional dihydrofolate reductase-thymidylate synthase (Marseillevirus ORF429)

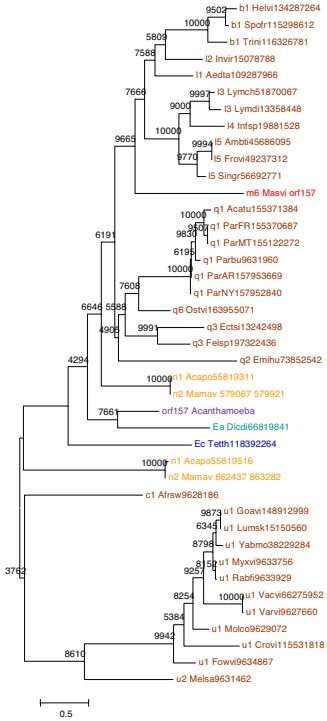

Fig. S4.26. Pox A32 (Marseillevirus ORF157)

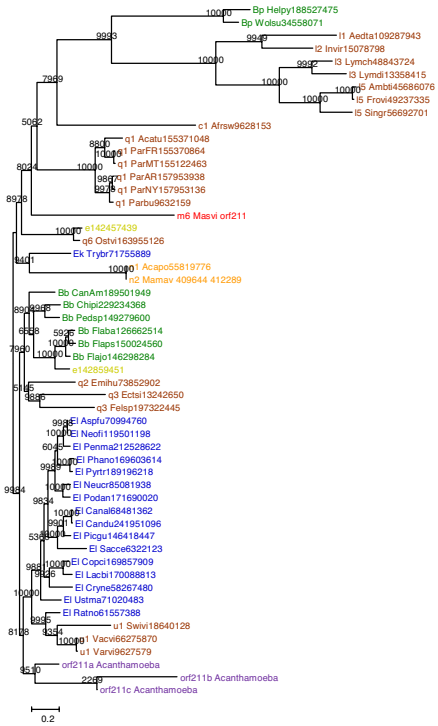

Fig. S4.27. helicase origin-binding-protein (UL9) like (Marseillevirus ORF211)

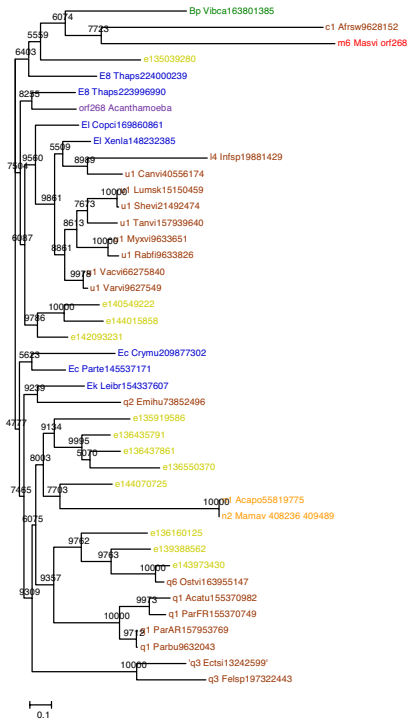

Fig. S4.28. Ribonucleotide reductase, small chain (Marseillevirus ORF268)

Fig. S4. Continued.

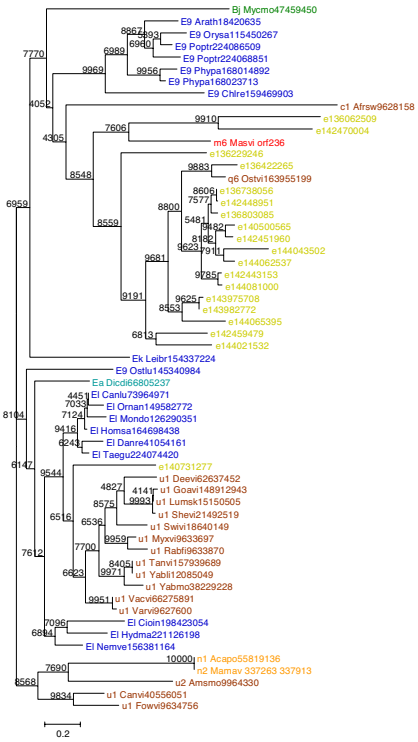

Fig. S4.29. Thymidine kinase (Marseillevirus ORF236)

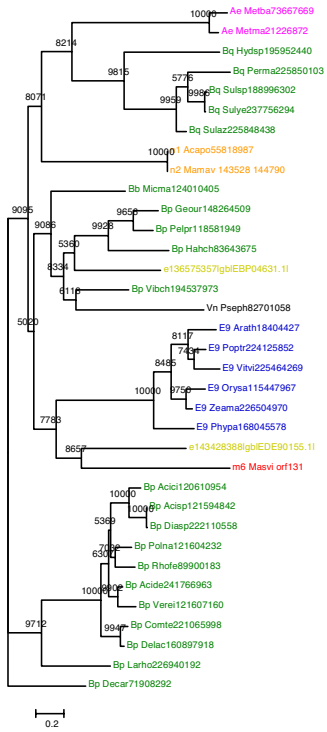

Fig. S4.30. DHH family phosphohydrolase (Marseillevirus ORF131)

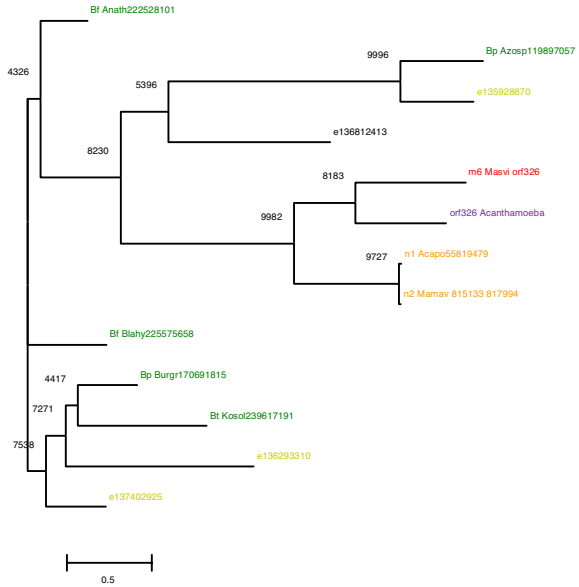

Fig. S4.31. P-loop ATPase or GTPase (Marseillevirus ORF326)

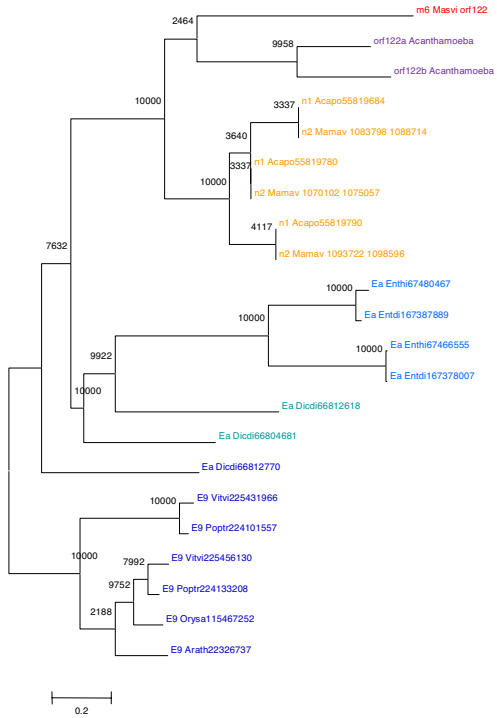

Fig. S4.32. Tandem kinase unique to Marseillevirus and Mamavirus (Marseillevirus ORF122)

Fig. S4. Continued.

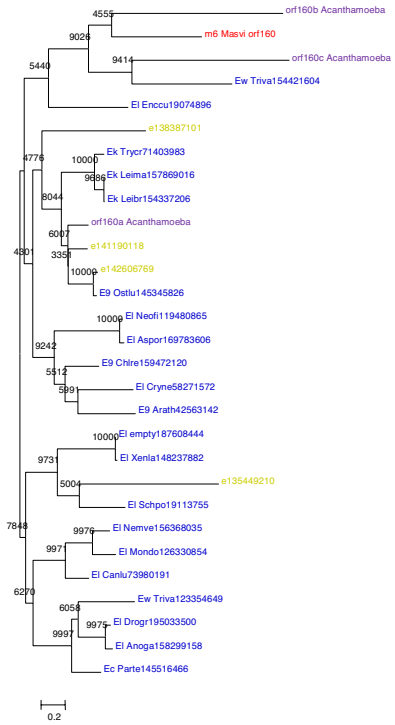

Fig. S4.33. Marseillevirus ORF160

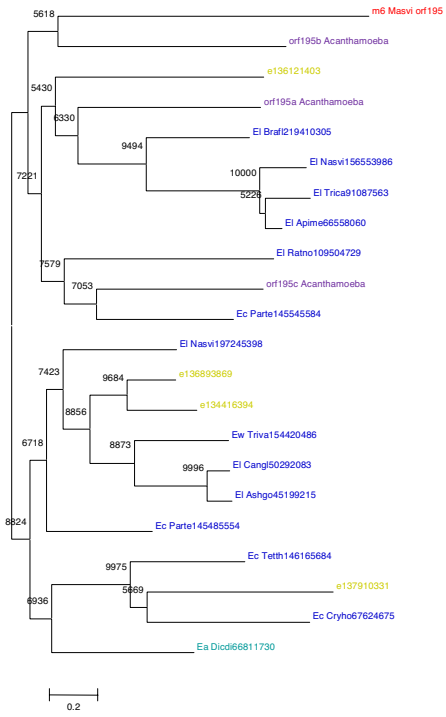

Fig. S4.34. Marseillevirus ORF195

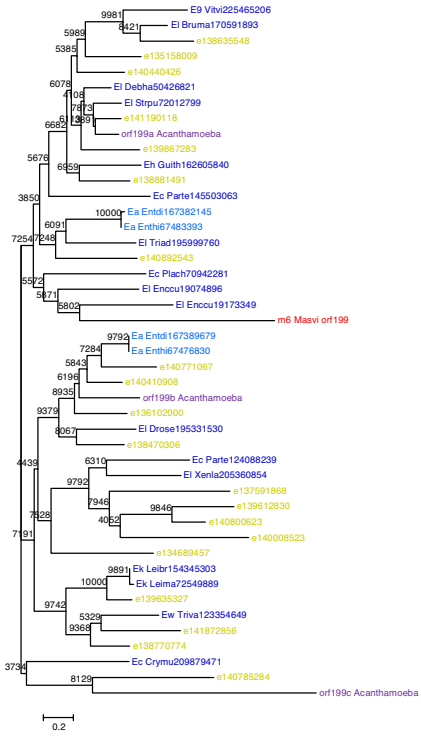

Fig. S4.35. Marseillevirus ORF199

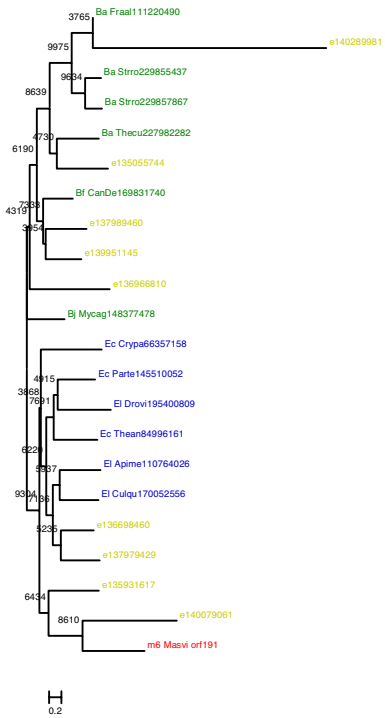

Fig. S4.36. Marseillevirus ORF191

Fig. S4. Continued.

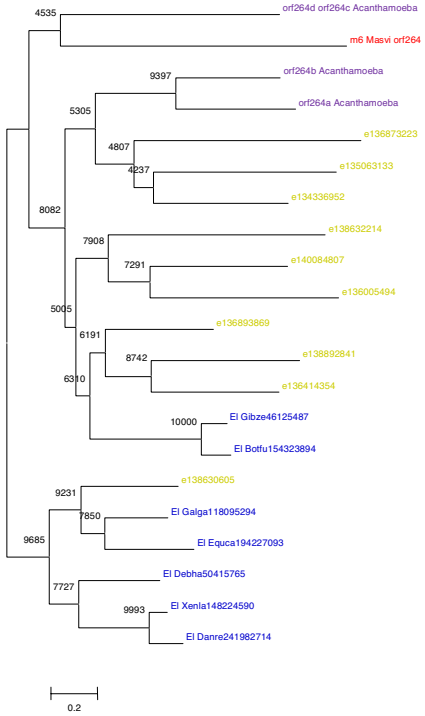

Fig. S4.37. Marseillevirus ORF264

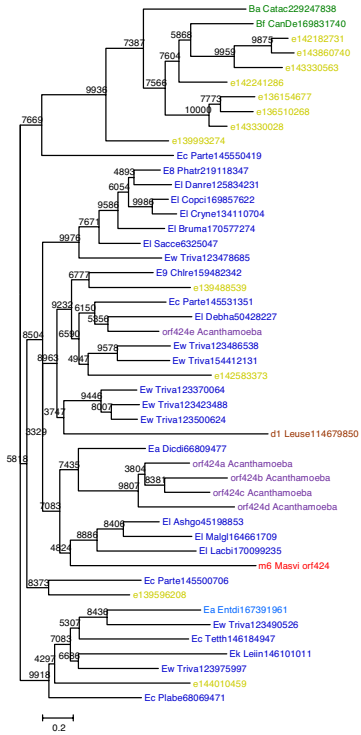

Fig. S4.38. Marseillevirus ORF424

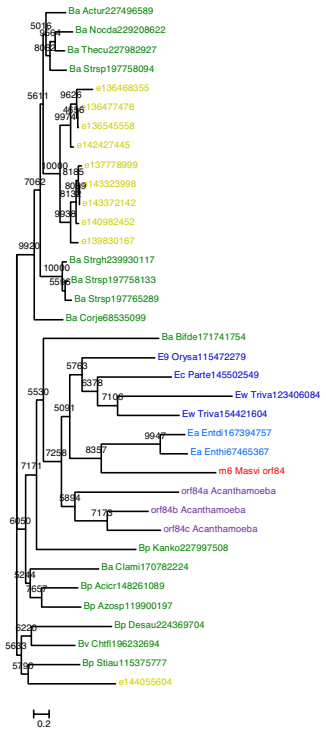

Fig. S4.39. Marseillevirus ORF84

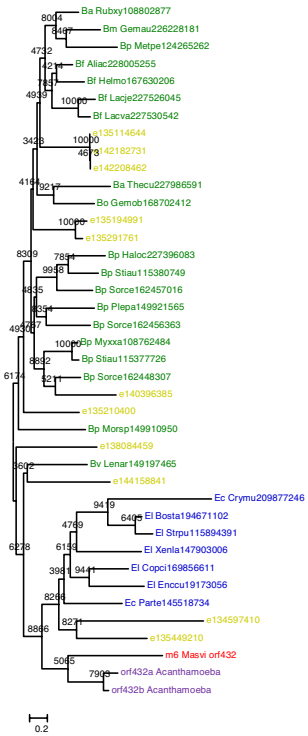

Fig. S4.40. Marseillevirus ORF432

Fig. S4. Continued.

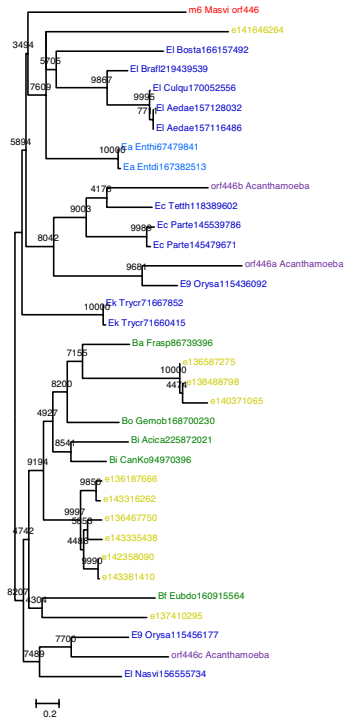

Fig. S4.41. Marseillevirus ORF446

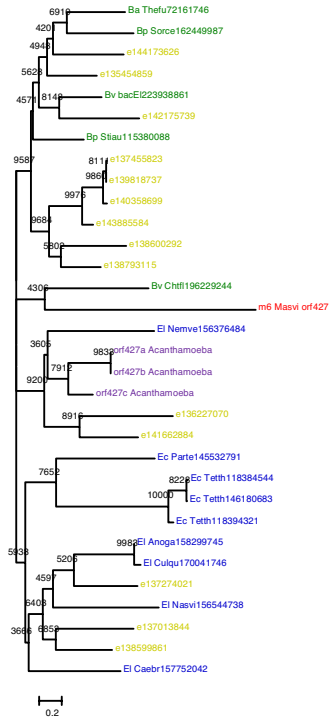

Fig. S4.42. Marseillevirus ORF427

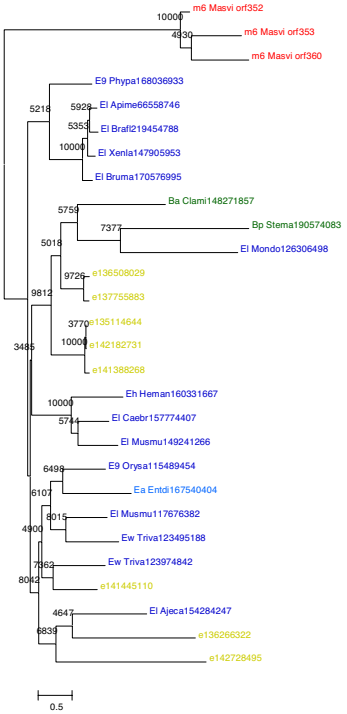

Fig. S4.43. Marseillevirus ORF352

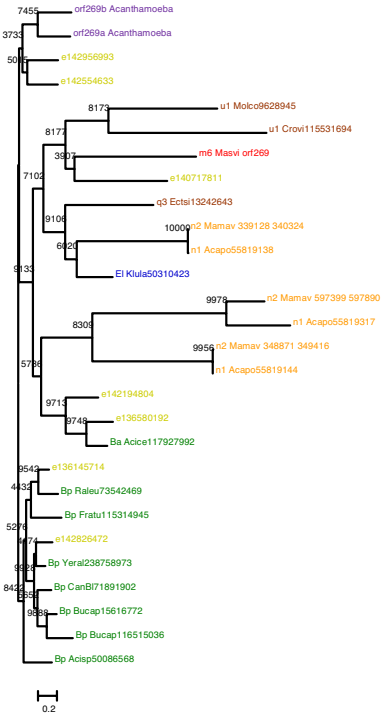

Fig. S4.44. chaperone protein DnaJ (Marseillevirus ORF269)

Fig. S4. Continued.

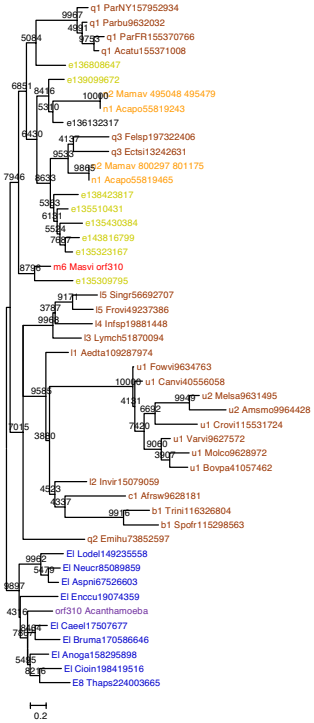

Fig. S4.45. Erv1/Alr family protein (poxvirus E10 ortholog) (Marseillevirus ORF310)

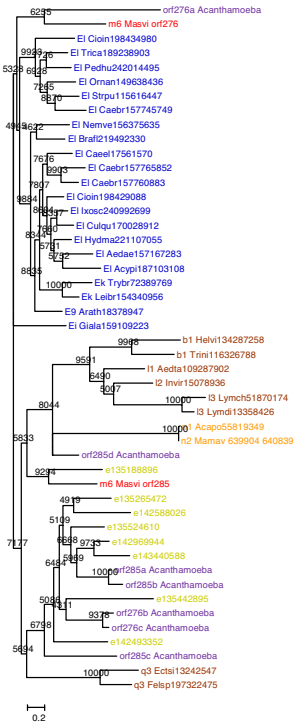

Fig. S4.46. papain-like cysteine peptidase (Marseillevirus ORF285)

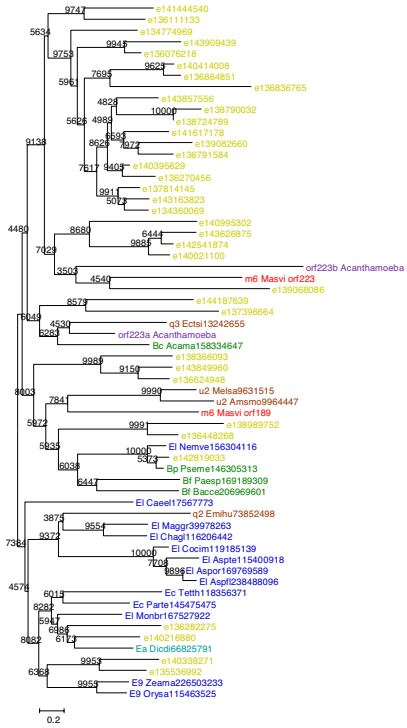

Fig. S4.47. Lipase class 3 (Marseillevirus ORF189)

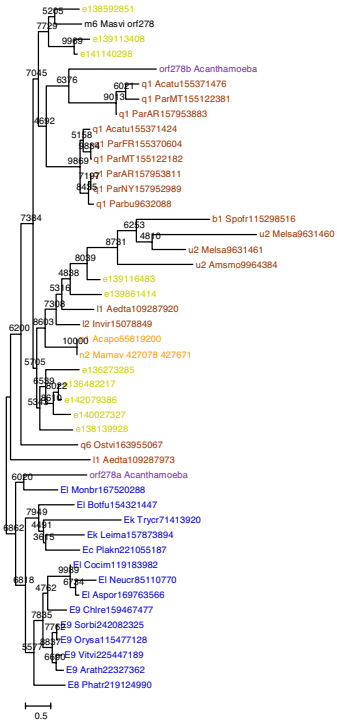

Fig. S4.48. metallopeptidase WLM (Marseillevirus ORF278)

Fig. S4. Continued.

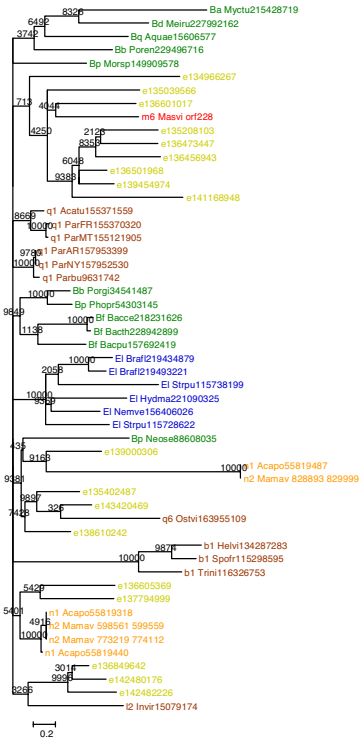

Fig. S4.49. Patatin-like phospholipase (Marseillevirus ORF228)

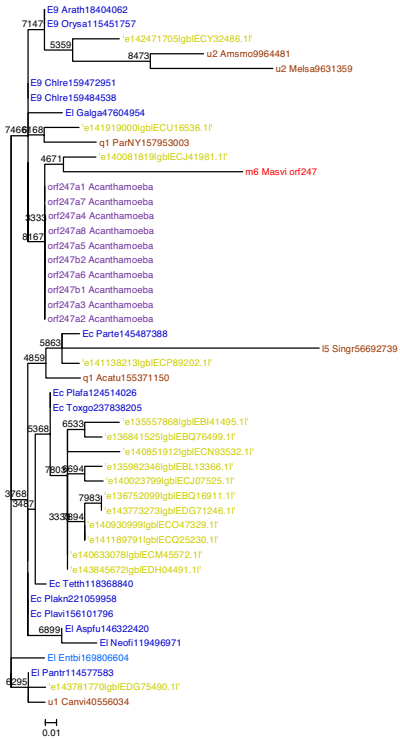

Fig. S4.50. Ubiquitin (Marseillevirus ORF247)

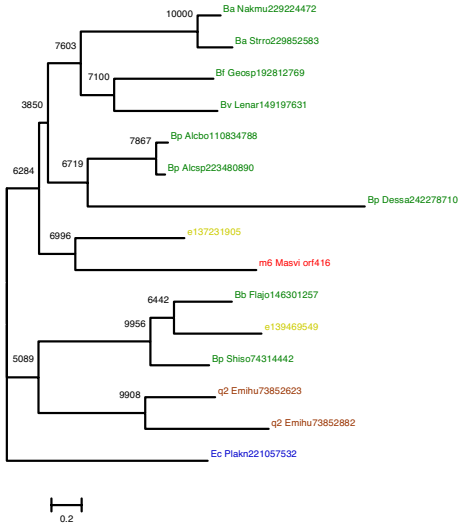

Fig. S4.51. peptidoglycan peptidase (Marseillevirus ORF416)

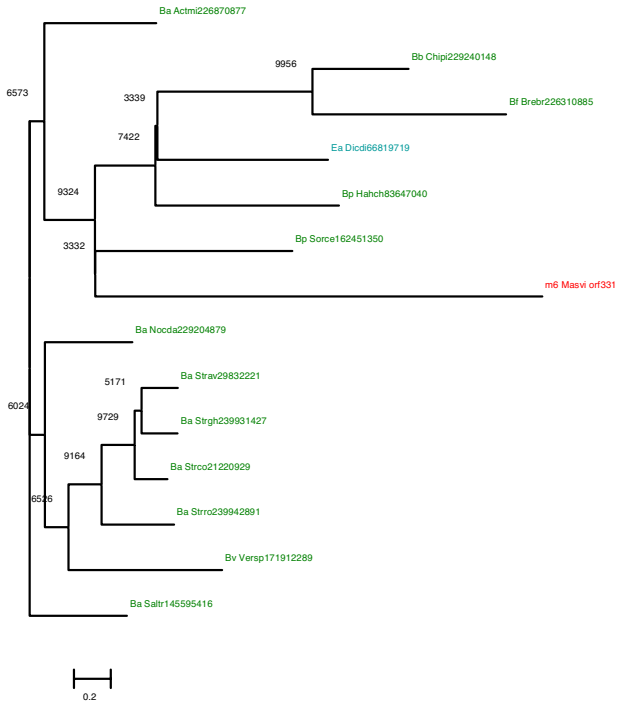

Fig. S4.52. ankyrin repeat protein (Marseillevirus ORF331)

Fig. S4. Continued.

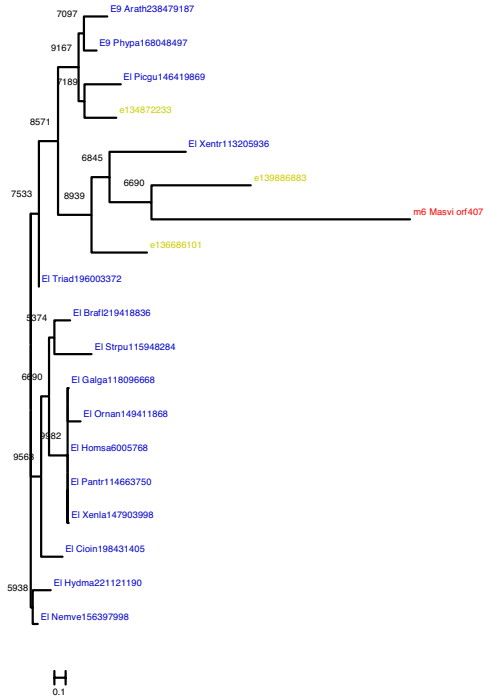

Fig. S4.53. ubiquitin-like protein (Marseillevirus ORF407)

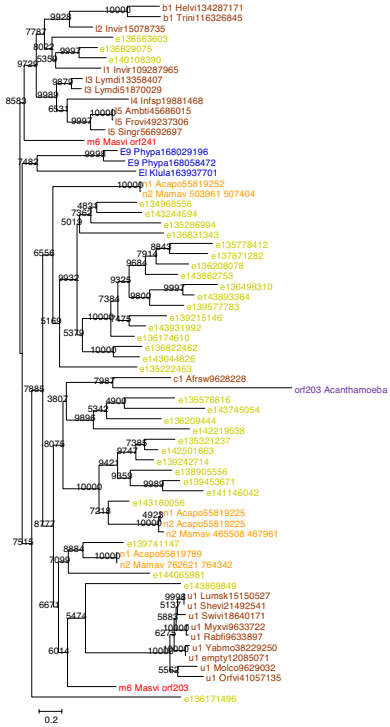

Fig. S4.54. D6/D11-like helicase (Marseillevirus ORF203)

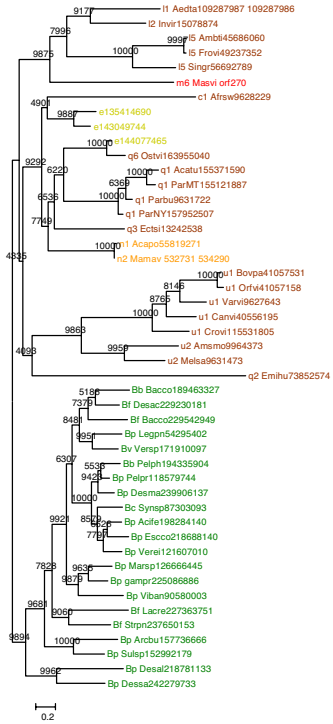

Fig. S4.55. helicase of superfamily II (Marseillevirus ORF270)

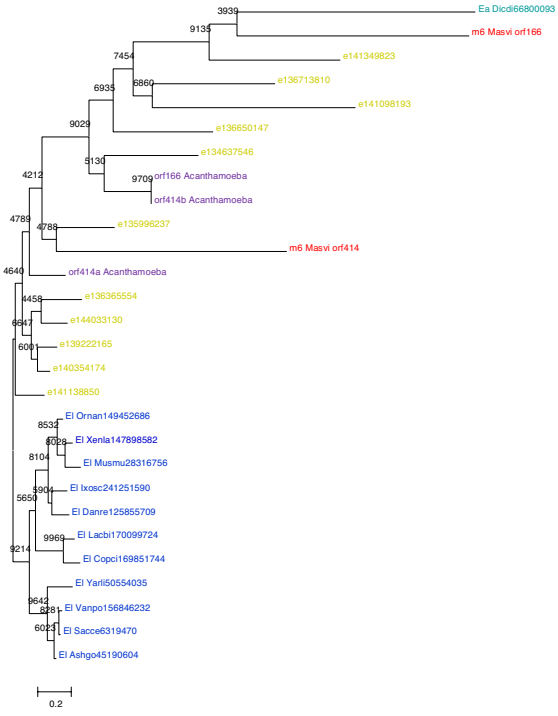

Fig. S4.56. Histone 2A-domain-containing protein (Marseillevirus ORF166)

Fig. S4. Continued.

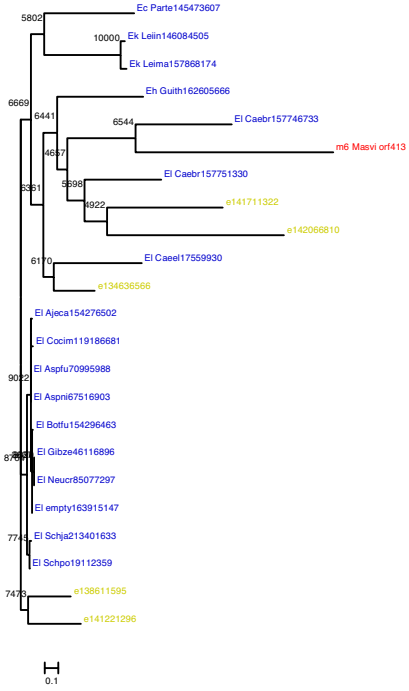

Fig. S4.57. Histone H3 (Marseillevirus ORF413)

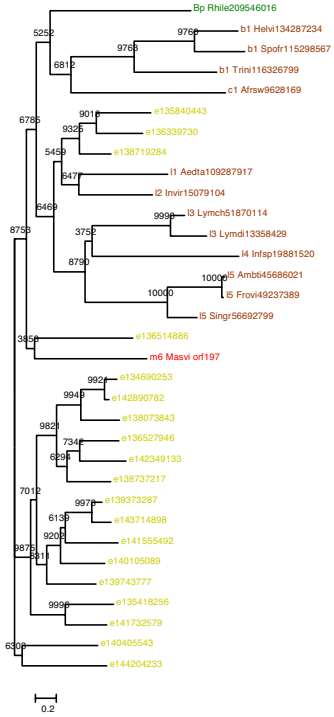

Fig. S4.58. RNA ligase (Marseillevirus ORF197)

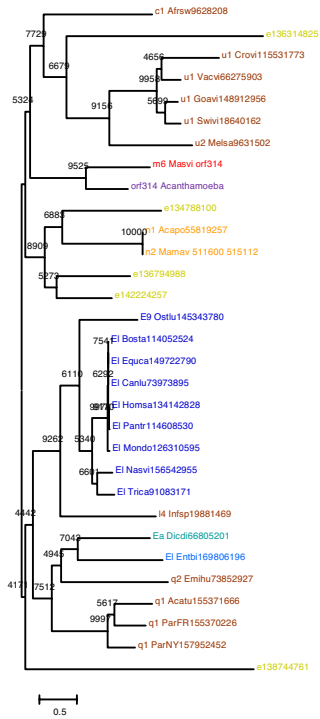

Fig. S4.59. 3-domain mRNA capping enzyme (Marseillevirus ORF314)

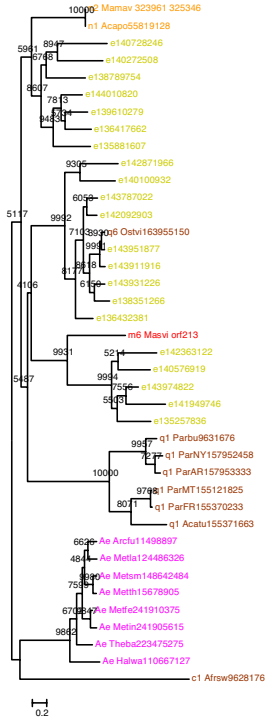

Fig. S4.60. Transcription initiation factor TFIIB (Marseillevirus ORF213)

Fig. S4. Continued.

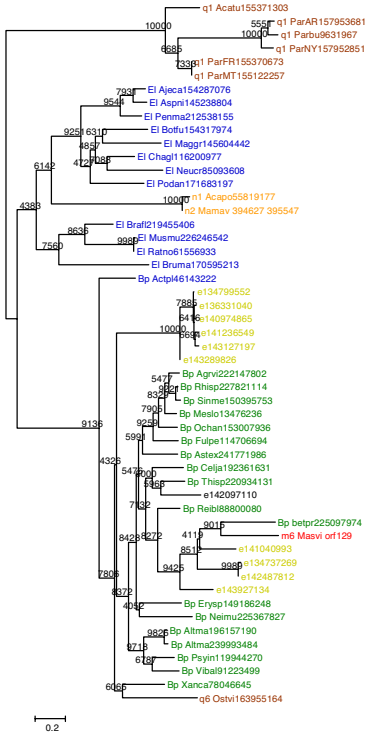

Fig. S4.61. ribonuclease H (Marseillevirus ORF129)

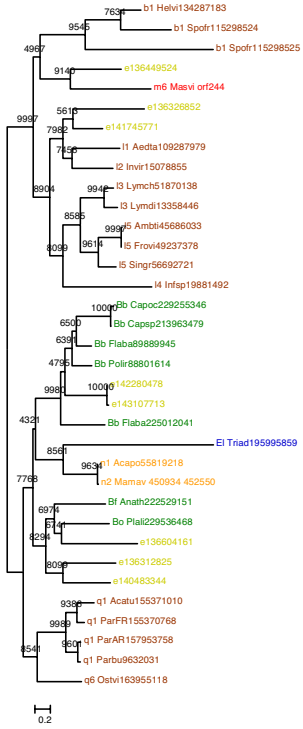

Fig. S4.62. ribonuclease III (Marseillevirus ORF244)

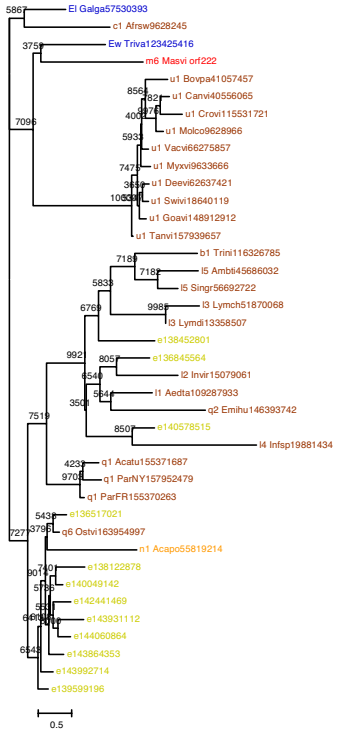

Fig. S4.63. Transcription factor S-II (TFIIS)-domain-containing protein, RNAP subunit (Marseillevirus ORF222)

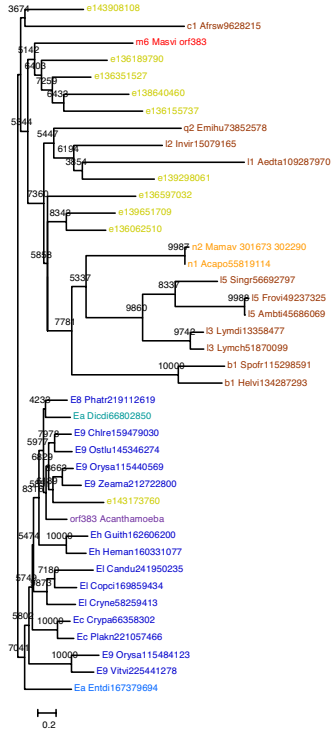

Fig. S4.64. RNAP subunit Rpb5 (Marseillevirus ORF383)

Fig. S4. Continued.

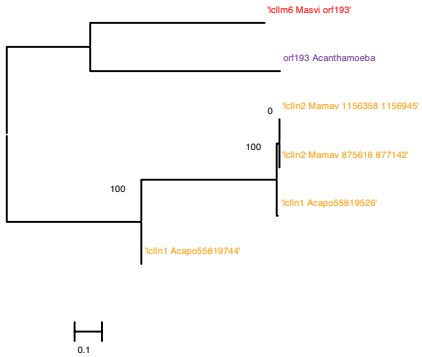

Fig. S4.65. multiple Zn fingers (Marseillevirus ORF193)

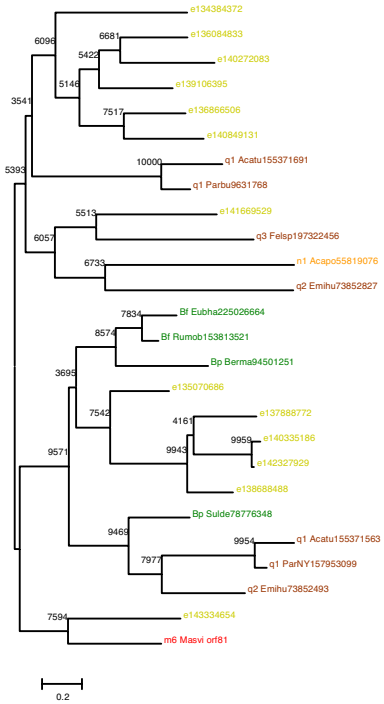

Fig. S4.66. Zn-ribbon-like motif (Marseillevirus ORF81)

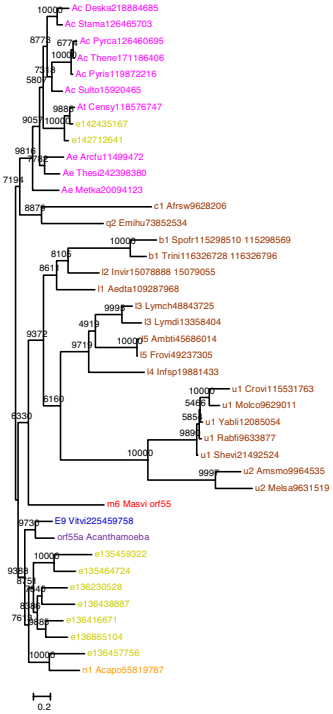

Fig. S4.67. DNA-directed RNA polymerase subunit alpha; RNA polymerase Rpb1, domains 3-7 (Marseillevirus ORF55)

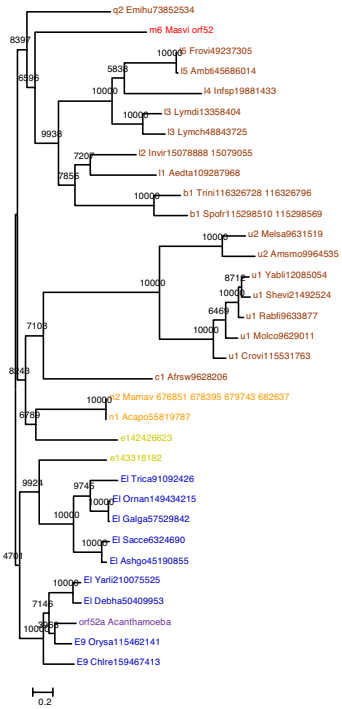

Fig. S4.68. DNA-directed RNA polymerase subunit alpha; RNA polymerase Rpb1, domains 1-2 (Marseillevirus ORF52)

Fig. S4. Continued.

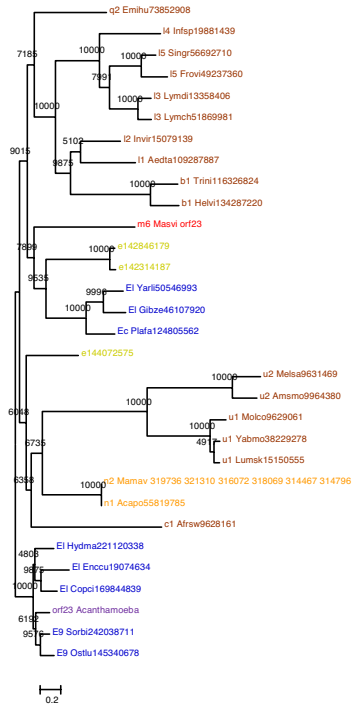

Fig. S4.69. DNA-directed RNA polymerase subunit beta (Marseillevirus ORF23)

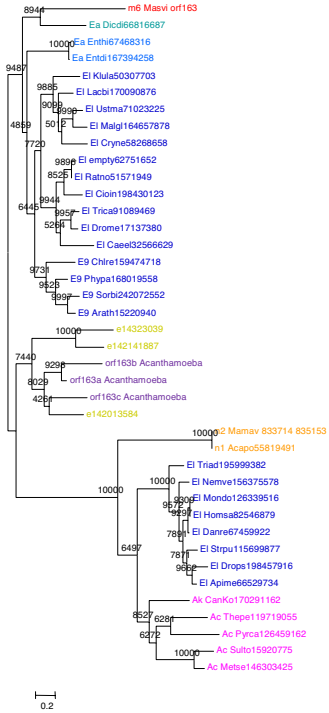

Fig. S4.70. Translation elongation factor EF-1alpha (Marseillevirus ORF163)

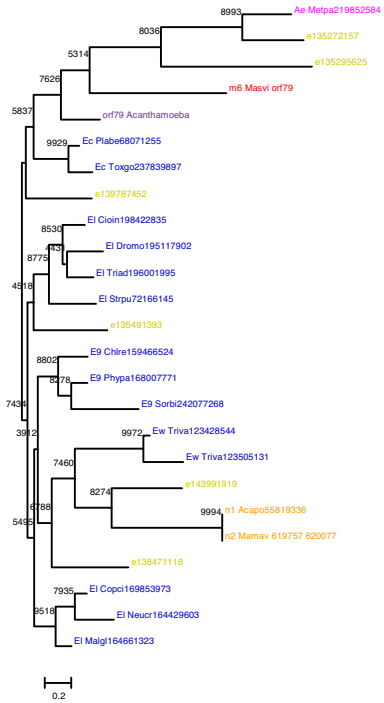

Fig. S4.71. Translation initiation factor SUI1 (Marseillevirus ORF79)

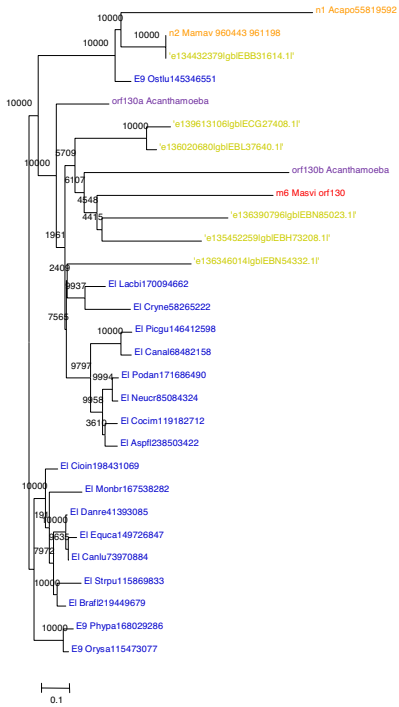

Fig. S4.72. Eukaryotic peptide chain release (translation termination) factor 1 (Marseillevirus ORF130)

Fig. S4. Continued.

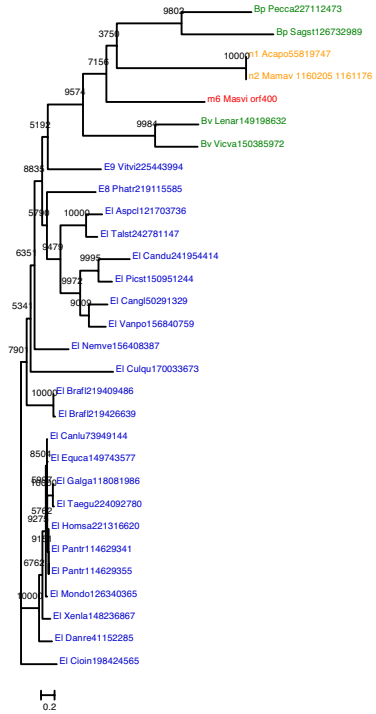

Fig. S4.73. cell division cycle 123 homolog (Marseillevirus ORF400)

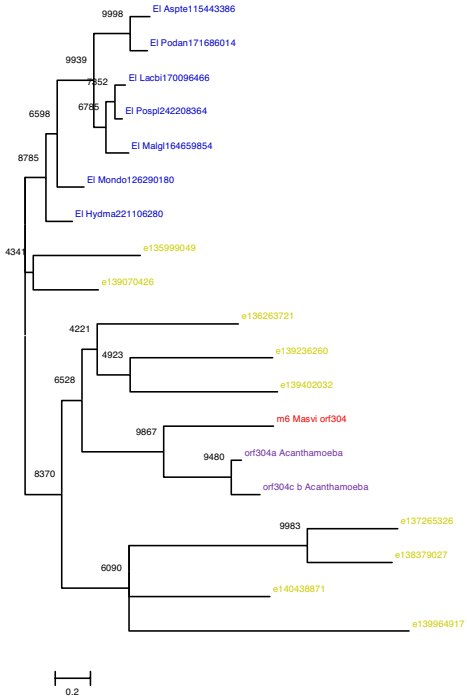

Fig. S4.74. eukaryotic translation initiation factor 5 (Marseillevirus ORF304)

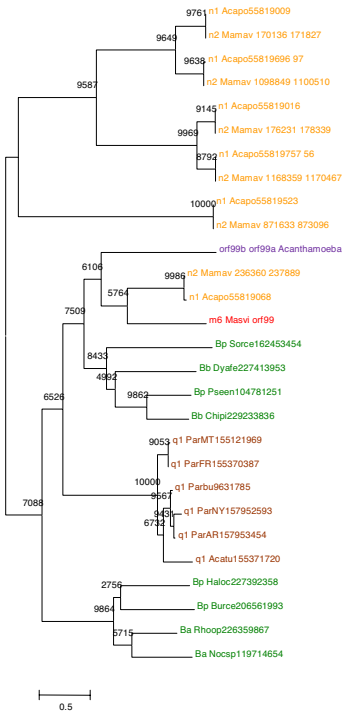

Fig. S4.75. Flavin-containing amine oxidoreductase (Marseillevirus ORF99)

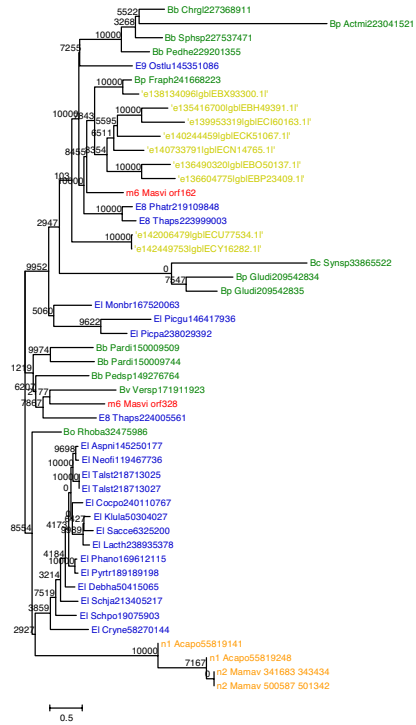

Fig. S4.76. mannosyltransferase OCH1-like protein (Marseillevirus ORF162)

Fig. S4. Continued.

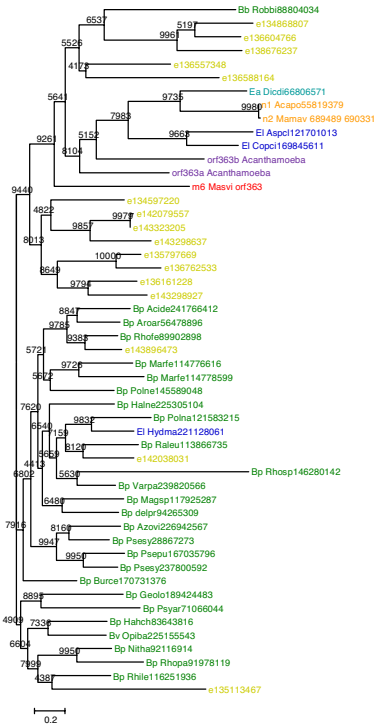

Fig. S4.77. calcineurin-like phosphoesterase (Marseillevirus ORF363)

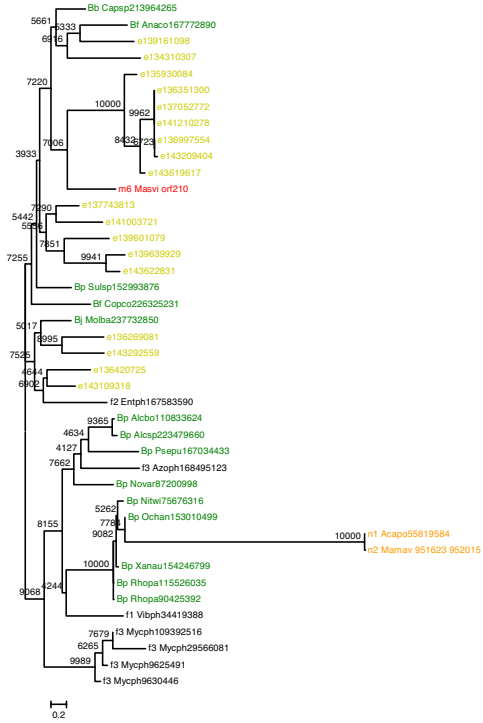

Fig. S4.78. Rossmann-fold nucleotide-binding protein (Marseillevirus ORF210)

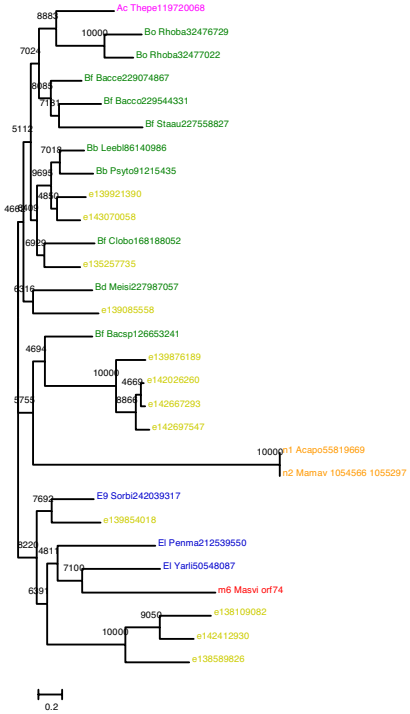

Fig. S4.79. Metal dependent phosphohydrolase with conserved 'HD' motif (Marseillevirus ORF74)

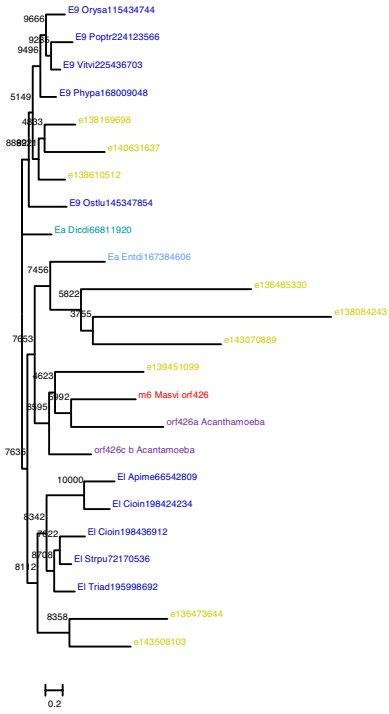

Fig. S4.80. WD repeat protein (Marseillevirus ORF426)

Fig. S4. Continued.

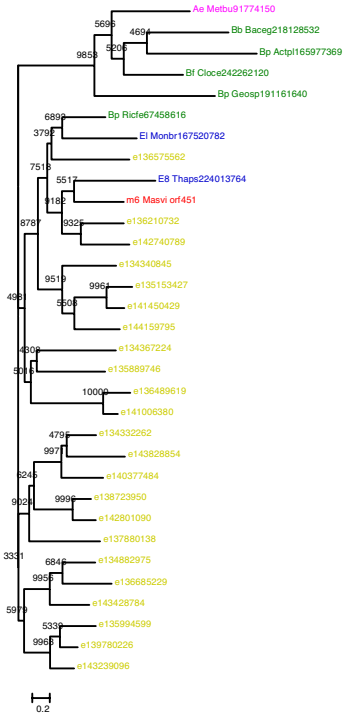

Fig. S4.81. glycosyltransferase (Marseillevirus ORF451)

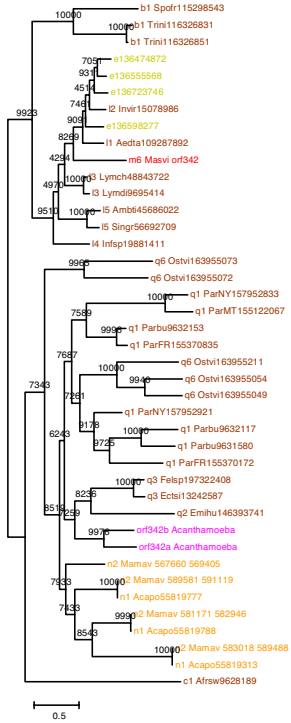

Fig. S4.82. major capsid protein (Marseillevirus ORF342)

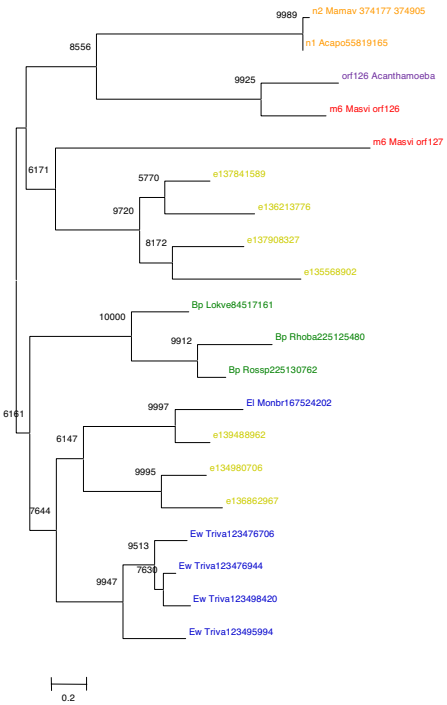

Fig. S4.83. uncharacterized protein conserved in several bacteria and eukaryotes, and mimivirus (low similarity) (Marseillevirus ORF126)

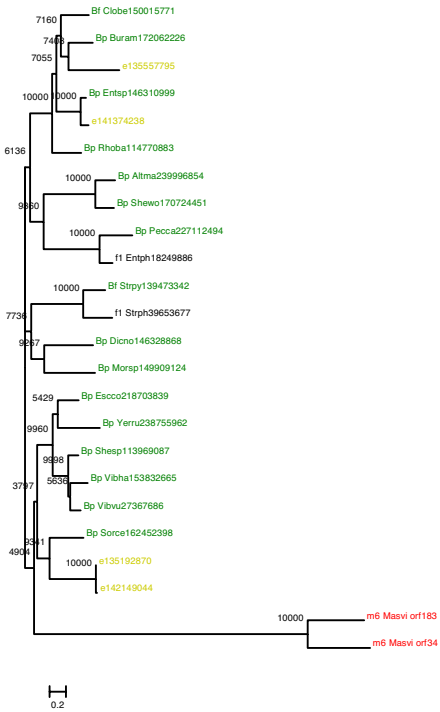

Fig. S4.84. contains an uncharacterized conserved domain found in diverse bacterial and phage proteins (Marseillevirus ORF183)

Fig. S4. Continued.

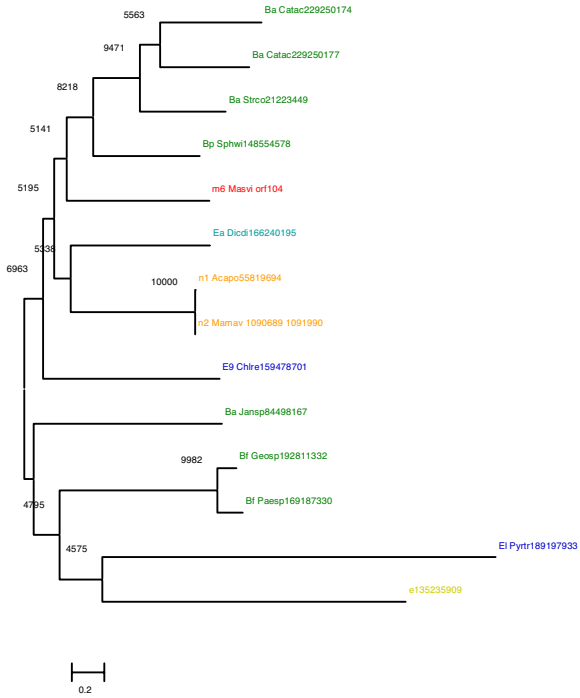

Fig. S4.85. Uncharacterized protein conserved in bacteria and mimivirus (Marseillevirus ORF104)

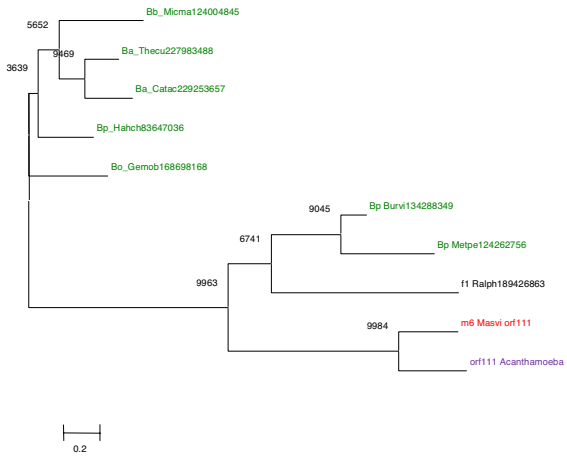

Fig. S4.86. uncharacterized protein with homologs in some bacteria (Marseillevirus ORF111)

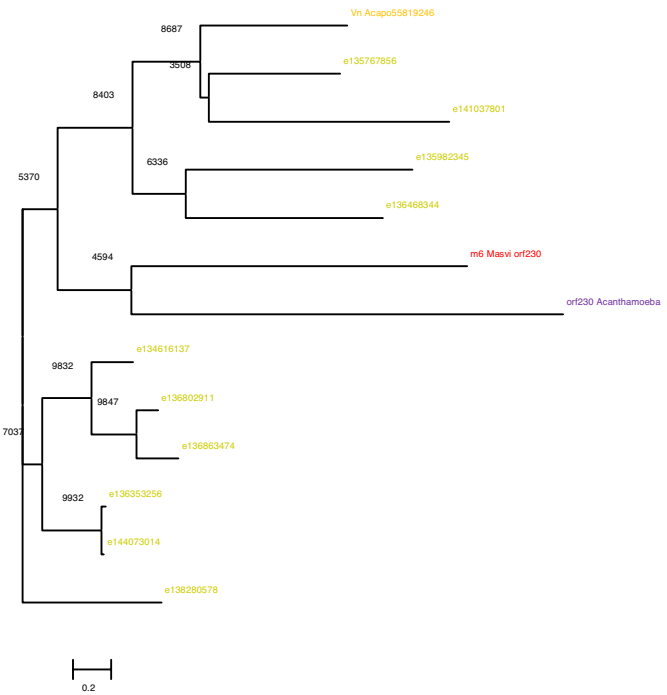

Fig. S4.87. uncharacterized, conserved domain in MIMI_L371 (Marseillevirus ORF230)

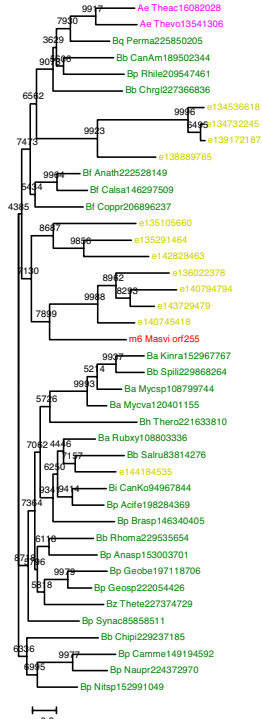

Fig. S4.88. uncharacterized TIM-barrel protein conserved in numerous bacteria (Marseillevirus ORF255)

Fig. S4. Continued.

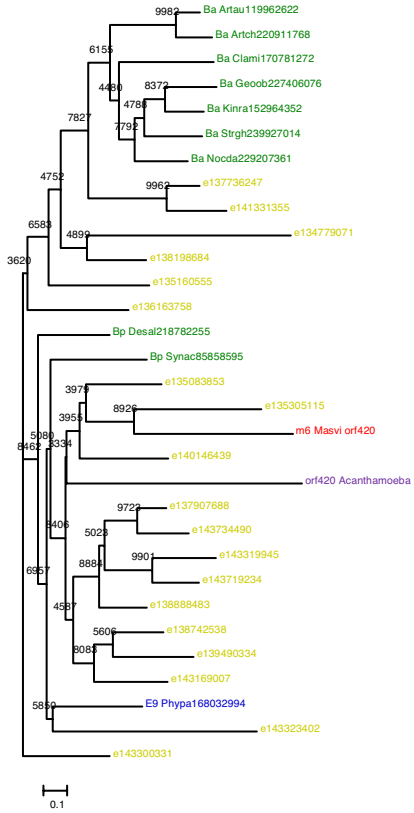

Fig. S4.89. uncharacterized protein conserved in bacteria and archaea (Marseillevirus ORF420)

Fig. S4. Continued.

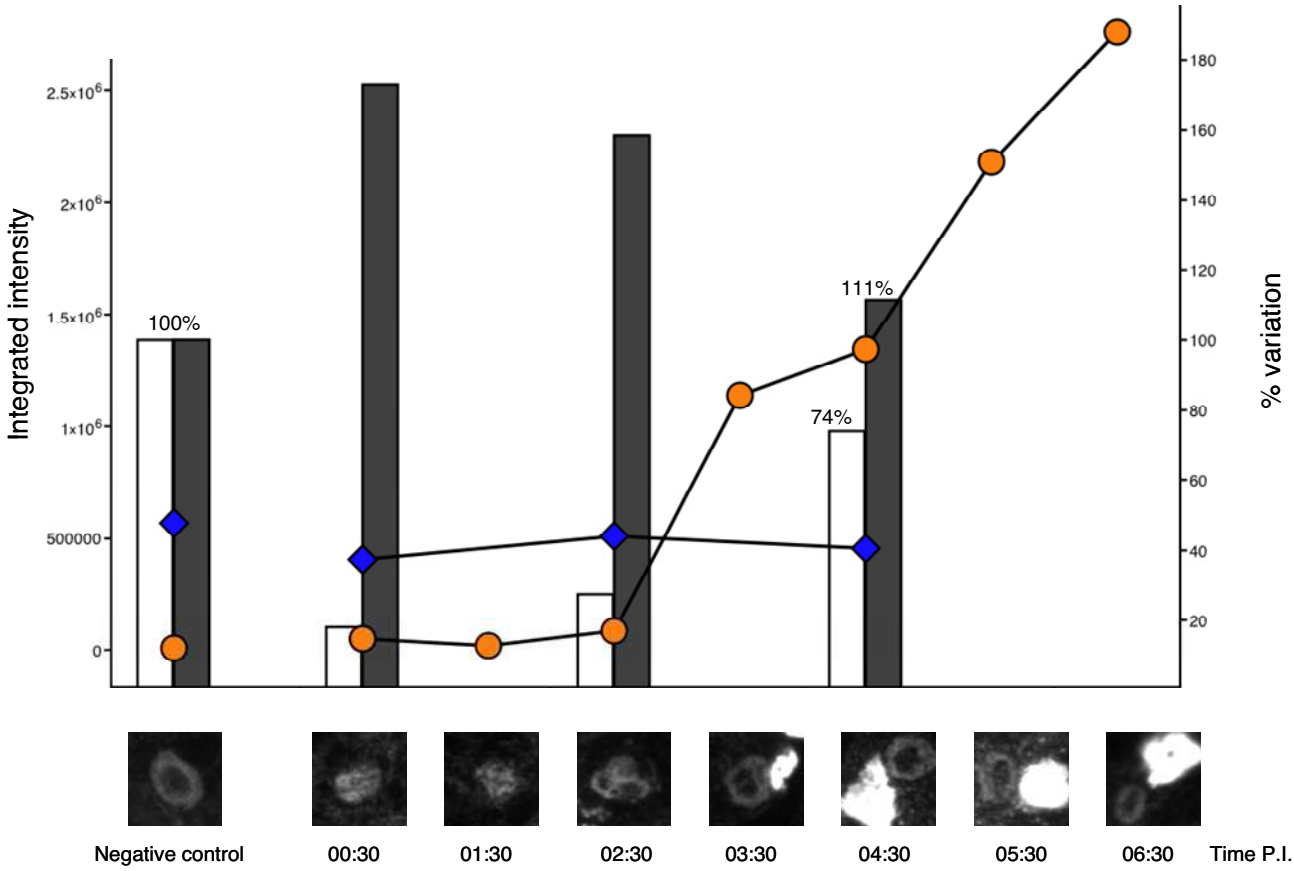

Fig. S5. Kinetics and quantification of Marseillevirus virus factory formation. Uninfected (negative control) or Marseillevirus infected *A. castellanii* at different times postinfection were stained with DAPI. Immunofluorescence pictures were taken using a 100× magnification lens. Evolution of virus factory (diamonds) was compared with cell nuclei (circles) mean DAPI intensity staining. Transient modification of cell nuclei morphology was expressed as the ratio variation of ring pattern nuclei/modified nuclei normalized to the negative control value (100% value) (white bars). Heterogeneity of cell nuclei DAPI staining was expressed as the standard deviation normalized to the negative control (100% value) (black bars).

Other Supporting Information Files

Table S1 (PDF)
Table S2 (PDF)
Table S3 (PDF)
Table S4 (PDF)